



HAL
open science

Effects of temperature and addition of zinc carboxylate to grease on the tribological properties of PA66 in contact with carbon steel

T. Kunishima, S. Nagai, T. Kurokawa, J. Galipaud, G. Guillonueau, G. Bouvard, J.-Ch. Abry, C. Minfray, V. Fridrici, Ph. Kapsa

► To cite this version:

T. Kunishima, S. Nagai, T. Kurokawa, J. Galipaud, G. Guillonueau, et al.. Effects of temperature and addition of zinc carboxylate to grease on the tribological properties of PA66 in contact with carbon steel. Tribology International, 2021, 153, pp.106578-. 10.1016/j.triboint.2020.106578 . hal-03491359

HAL Id: hal-03491359

<https://hal.science/hal-03491359>

Submitted on 30 Aug 2022

HAL is a multi-disciplinary open access archive for the deposit and dissemination of scientific research documents, whether they are published or not. The documents may come from teaching and research institutions in France or abroad, or from public or private research centers.

L'archive ouverte pluridisciplinaire **HAL**, est destinée au dépôt et à la diffusion de documents scientifiques de niveau recherche, publiés ou non, émanant des établissements d'enseignement et de recherche français ou étrangers, des laboratoires publics ou privés.



Distributed under a Creative Commons Attribution - NonCommercial 4.0 International License

Effects of temperature and addition of zinc carboxylate to grease on the tribological properties of PA66 in contact with carbon steel

T. Kunishima^{a,b}, S. Nagai^a, T. Kurokawa^a, J. Galipaud^b, G. Guillonau^b, G. Bouvard^b, J.-Ch. Abry^b, C. Minfray^b, V. Fridrici^b, Ph. Kapsa^b

^a JTEKT CORPORATION, 333 Toichi-cho, Kashihara, Nara 634-8555, Japan

^b Laboratoire de Tribologie et Dynamique des Systèmes, UMR CNRS 5513, Ecole Centrale de Lyon, Université de Lyon-36 avenue Guy de Collongue F-69134 Ecully cedex, France

Corresponding author: Takeshi Kunishima E-mail: takeshi_kunishima@jtekt.co.jp

Keywords: Polyamide, Glass fibers, Grease, Zinc carboxylate

ABSTRACT

In this study, the influence of temperature on the tribological properties of unreinforced or glass-fiber reinforced PA66 in contact with carbon steel under boundary lubrication with grease was studied when considering the temperature dependence of the mechanical properties on the sliding surface of PA66 and the tribochemical reaction to zinc carboxylate additives in grease. XPS and ToF-SIMS analyses revealed the formation of a carboxylate tribofilm on the steel surface and a zinc sulfide reactive film on the PA66 surface, which are related to the tribochemical reaction of the additives present in the grease applied. The formation of the tribofilm contributed to an improvement of the tribological properties, particularly at 80 °C.

1. Introduction

Polyamide 66 (PA66) has interesting properties, including heat resistance, a high strength, toughness, and good wear resistance [1–5], and is therefore widely used for sliding parts in automobiles or industrial machines, such as gears [6–12] and bearing retainers [13–15]. Unreinforced PA66, which does not contain reinforcement fibers, is used for sliding parts [16–18]. In addition, reinforcement fibers such as glass fibers (GFs) or carbon fibers (CFs) may be added to PA66 to increase its strength and stiffness, and thus meet the requirements for a downsizing of parts under severe conditions [19–24]. To use such parts under a high-temperature environment, such as inside an engine compartment of an automobile, it is necessary to understand the temperature dependence of the tribological properties. Shin et al. [23] reported the effects of temperature on the tribological properties of unreinforced PA66 in contact with carbon steel under dry conditions. The friction coefficient and wear rate of PA66 increased owing to a degradation in the mechanical properties of resin and an increased adhesion to a counterbody surface at high temperatures. However, the majority of previous studies focusing on the tribology of polyamide have been conducted under dry conditions, and very few studies have focused on the temperature dependence of the tribological properties of PA66 under grease lubrication. Grease lubrication is a common way to decrease the friction of sliding parts under high contact pressure, thereby lowering the sliding heat, such as in the sliding of a resin worm gear and a metallic worm shaft used in a worm reducer of an electric power steering system of an automobile [25–27]. In the authors' previous study [28], the tribological properties

of carbodiimide-added GF or aramid fiber (AF) reinforced PA66 in contact with steel under a barium-complex based grease lubrication were investigated. The wear resistance of a PA66 composite was improved by an increase in the molecular weight of PA66 through the reactive extrusion between PA66 and poly-carbodiimide compounds. Bormuth et al. [29] reported the effects of various grease compositions on the efficiency and temperature in small plastic gears comprising a steel worm shaft and PA66 gear wheel. They determined that the viscosity of the base oils and the applied load have a significant effect on the friction torque. In addition, a polytetrafluoroethylene (PTFE) type thickener shows a significant increase in efficiency compared to a lithium-soap thickener when using PAO-based grease. Kochi et al. [30] attempted to measure the thickness of a soft EHL film and the traction of oil and grease using an optical interferometry system, in which a steel ball is placed in contact with a transparent polycarbonate disk with a Young's modulus close to that of engineering plastic, such as polyamide. A soft EHL film with grease is thicker than a film with its base oil, as is the case of a hard EHL film. The film thickness with grease changes with different thickeners depending on its apparent viscosity, as estimated using the Bauer model. Kurokawa et al. [31] reported the tribological properties of a spur gear made of CF-reinforced poly-ether-ether-ketone (PEEK) under lithium grease lubrication, with a counterpart of CF-reinforced PEEK or steel. The authors found that the affinity between PEEK and CF, and the characteristics of CF (namely, the strength and modulus of the fibers) play a significant role in determining the wear resistance of the composite. However, in previous studies on the tribology of polyamide or other types of engineering plastic in contact with steel under grease lubrication, the temperature dependence on the tribological properties, or the detailed mechanism of the tribochemistry, on the sliding surface have yet to be clearly discussed.

The effects of additives on a tribochemical reaction related to grease have been shown to be significant. Oiliness improvers, anti-wear agents, friction modifiers, and extreme pressure agents are well-known additives for improving the tribological properties. Oiliness improvers are used to decrease the friction and wear by the formation of an oil adsorption film on the sliding surface, particularly under low normal loading conditions. Long chain fatty acids, fatty acid esters, and long chain alcohols are known examples of oiliness improvers [32–36]. An anti-wear agent is a load-bearing additive that reacts with a metallic surface to form another film when the oil film or oxidation-protective film on the metallic surface breaks under a high load or low speed conditions, and prevents the direct contact of the sliding surface. Examples of an anti-wear agent include metal dialkyldithiophosphate including antimony and zinc such as zinc dialkyldithiophosphate (ZnDTP), or phosphate and thiophosphate esters, such as tricresyl phosphate, di-n-octyl phosphite, or isodecyl diphenyl phosphite [32, 37–39]. Friction modifiers act through the tribochemical formation of a low friction film. Molybdenum dithiocarbamate (MoDTC) is one example, leading to the formation of a molybdenum disulfide (MoS_2) tribofilm [37–39]. Extreme pressure additives are used to prevent a seizure or scuffing under extreme pressure lubrication at high temperature. Organic sulfur, phosphorus compounds, and organic halogen compounds are known to operate as extreme pressure additives [32, 40]. Previous studies have focused on the mechanism of tribochemistry on the sliding surface of steel, ceramic, or hard coatings (such as diamond-like carbon), and on the effects of the tribological properties when using such additives. However, regarding the sliding of polymer and steel, or the sliding between polymers, few studies have been conducted on the tribochemistry of the

additives or on the effects of a tribofilm formation on the tribological properties.

Considering these backgrounds, in this study the effects of adding zinc carboxylate to grease on the tribological properties of unreinforced or GF-reinforced-PA66 in contact with carbon steel under boundary lubrication were investigated. Zinc carboxylate is a type of oiliness improver and is considered to work more effectively as a low friction agent under lower contact pressure conditions in the sliding of PA66 and steel than in the sliding between steel sheets [32, 41]. In addition, zinc carboxylate has a good affinity with PA66 [41]. First, the effects on the tribological properties of GF-reinforced PA66 when adding zinc carboxylate to grease at different temperatures were investigated. Next, the composition of a tribofilm on steel and a PA66 surface was identified through a chemical analysis, and the effects of the tribofilm formation on the tribological properties are discussed herein.

2. Experimental

2.1 PA66 material

Sliding test specimens of unreinforced PA66 were prepared through injection molding using pellets (granules) of commercially available PA66 with normal level of molecular mass. To prepare for specimens composed of a GF-reinforced PA66 composite, the same unreinforced PA66 was used for extrusion to prepare for the pellets as in the authors' previous work [28, 42]. GFs with the diameter of 6.5 μm were chopped to the length of 3 mm. Good adhesion between the PA66 and GF were ensured through the surface treatment agents of GF, as presented in a scanning electron microscopy (SEM) observation on the fracture surface after the tensile test using this composite material (Fig. 1). An extrusion of the PA66 and GF chopped strands was carried out. The GFs amounted to 15 wt%. The sliding test specimens described in Section 2.4 were prepared through the injection molding process of the obtained pellets. The Young's modulus was measured through a traction test following the standard ISO 527. Mechanical properties of the tested PA66 are listed in Table 1.

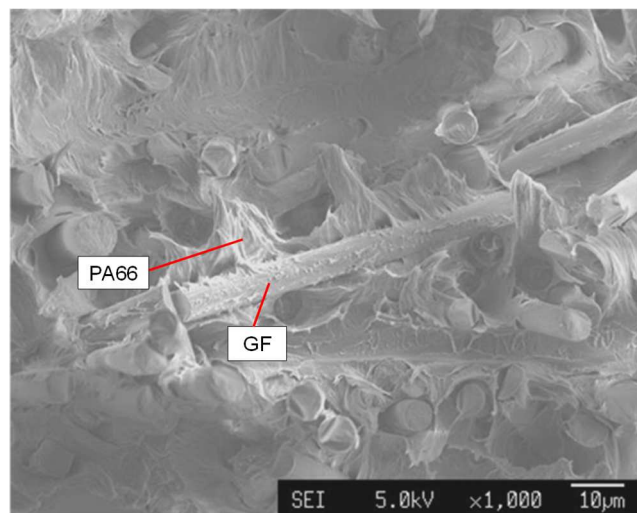


Fig. 1 SEM observation of the fracture surface after the tensile test using this composite material.

Table 1 Mechanical properties of evaluated PA66.

	Young's modulus at room temperature
Unreinforced PA66	3 GPa
GF-reinforced PA66	6 GPa

The ring specimens were cut in the height direction at 3 mm with a lathe, and the sliding surface was then polished with #600 polishing paper before each sliding test. The objective of this process is to simulate the conditions of the sliding surface of an actual worm gear tooth surface formed through mechanical hob-cutting after an injection molding process to ensure the dimensional stability, as well as GF exposure on the sliding surface.

The Young's modulus and hardness of the sliding surface of the GF-reinforced PA66 composite and unreinforced PA66 were measured based on the micro indentation at different temperatures. The micro indentation device used was developed by Alemnis [43] and can operate at up to 600 °C in an SEM. The heating procedure and temperature matching between the tip and sample used to conduct precise temperature tests at different temperatures are described in [44]. Experimental tests were conducted using a Berkovich tip made of tungsten carbide. The hardness and Young's modulus were both calculated using the Oliver–Pharr method [45]. Table 2 presents the measurement conditions. More particularly, the loading and unloading procedures were applied using a constant strain rate, which is important for time-dependent materials such as PA66 [46]. In addition, a strain of 0.2 s⁻¹ was chosen (high strain rate value) to avoid a nose formation in the unloading curve, preventing the unloading stiffness calculation [47]. Finally, the thermal drift was checked by applying a holding time at a constant load of 2 mN during 60 s.

Table 2 Micro indentation test conditions.

Tested material	GF composite	Unreinforced PA66
Type of indenter	Berkovich (WC)	Berkovich (WC)
Maximum normal load	500 mN	250 mN
Indentation test procedure	Loading strain rate \dot{P}/P : 0.2 s ⁻¹ Holding time at 500 mN: 10 s Unloading strain rate \dot{P}/P : 0.2 s ⁻¹ Holding time at 2 mN (checking thermal drift): 60 s	Loading strain rate \dot{P}/P : 0.2 s ⁻¹ Holding time at 250 mN: 10 s Unloading strain rate \dot{P}/P : 0.2 s ⁻¹ Holding time at 2 mN (checking thermal drift): 60 s
Temperature	25 °C, 80 °C, 120 °C	25 °C, 80 °C, 120 °C

2.2 Steel cylinders

Steel cylinders used for the sliding tests described in Section 2.4 with a diameter of 3.5 mm and a length of 30 mm were fabricated using S45C steel, which contains 0.45% carbon, following JIS G 4051. The roughness of

the sliding surface is $S_a = 0.18 \mu\text{m}$, which is obtained through a centerless grinding process. The Vickers hardness of the cross section of the cylinders is HV311, and the hardness of the cylinder surface measured by the micro indentation is 4.7 GPa.

2.3 Grease

The grease evaluated is composed of poly- α -olefin 8 (PAO8) as the base oil, diurea as a thickener, zinc carboxylate as a low friction agent, and an anti-oxidation agent containing sulfur compounds. The kinematic viscosity of PAO8 is $48 \text{ mm}^2/\text{s}$ at $40 \text{ }^\circ\text{C}$ and $8 \text{ mm}^2/\text{s}$ at $100 \text{ }^\circ\text{C}$. Diurea thickener was synthesized by the reaction of diisocyanate and several types of monoamine, and it was mixed to the base oil at specific rates. Zinc carboxylate is a mixture of different types of zinc carboxylates, including stearate, palmitate, and oleate. The added amounts of zinc carboxylate were in the range of 5-8 wt%, and the added amounts of sulfur type anti-oxidation agent were in the range of 0.5-3 wt% to the total composition of grease. The effects of the addition of each additive to grease were discussed based on an evaluation of the different types of grease applied. Table 3 lists the composition of each tested grease. The consistency (cone penetration) of the evaluated greases is 300.

Table 3 Composition of tested grease.

Sample number	Base oil	Thickener	Low friction agent	Anti-oxidation agent
No. 1	PAO8	Diurea	Zinc carboxylate	Sulfur type agent
No. 2	PAO8	Diurea	-	Sulfur type agent
No. 3	PAO8	Diurea	Zinc carboxylate	-

2.4 Experimental setup and measurements

Sliding tests using PA66 or composite ring and steel cylinders into contact under grease-lubricated conditions were conducted to evaluate the tribological properties. This test method is the originally devised one, which is the same tribological contact as applied in the authors' previous research [28, 42]. Fig. 2 illustrates a schematic view of the specimens used for the sliding test and tribometer. With this test setup, it is possible to simulate the contact geometry or pressure of actual worm gears. Intermittent sliding, repeating sliding duration and stopping duration, was introduced to reduce the sliding heat generation. The tests were conducted under grease lubricated conditions. 0.85 g of grease was supplied in and around the contact surface before each sliding test. A normal load was applied using dead weights. The weight of the ring before/after tests was measured through balance, and weight decrease (wear) of each ring specimen was estimated. In addition, the height of the ring before/after tests was measured through micrometer, and height decrease of each ring specimen was estimated. It allowed to estimate the wear and the creep separately, and to investigate the contributions of wear and creep in a sample. The total height loss h_{total} (which is the difference between the height of the composite ring before the test and the height of the composite ring after the test) is the total loss caused by wear and creep, whereas the wear height loss h_{wear} can be calculated from the wear mass of PA66 M_{wear} , the density of the PA66 d (1.14 g/cm^3 for unreinforced PA66 and 1.23 g/cm^3 for

GF-reinforced PA66), and the sliding surface area s (approximately 200 mm²) using the following equation:

$$h_{wear} = \frac{M_{wear}}{dS}. \quad (1)$$

The creep height loss h_{creep} was then estimated by subtracting the wear height loss from the total height loss.

$$h_{creep} = h_{total} - h_{wear} \quad (2)$$

In addition, the vertical displacement of the holder of the four steel cylinders was measured *in situ* during the sliding tests. However, this value was not exactly the same as the height loss of the PA66 ring measured before/after sliding tests because the PA66 ring specimens expanded owing to the heat generated by sliding during the tests and then contracted from the cooling after each test, and because of the possible contribution of wear of the steel cylinders. During our tests, the temperature of the steel cylinder holder was measured using a thermocouple, as presented in Fig. 2. The friction torque T was measured with a friction torque sensor, and the friction coefficient μ was calculated using the normal load N and the mean rotation radius r (11.4 mm).

$$\mu = \frac{T}{rN} \quad (3)$$

Friction torque was measured every 0.01 s, and the average and maximum values of the friction coefficient during a period of 1 s were calculated. One cycle in this sliding test represents one rotation of the PA66 ring. Table 4 lists the sliding test conditions. Two different conditions for the stopping duration were introduced: 1-s stopping conditions to conduct the test with a heat generation by sliding, and 200-s stopping conditions to conduct the test at a stable temperature by cooling during the long stopping phase. Two sliding tests were conducted under the same test conditions. Sliding tests were conducted under the boundary lubrication conditions considering the estimated oil film thickness and oil film parameter (details; see supplementary).

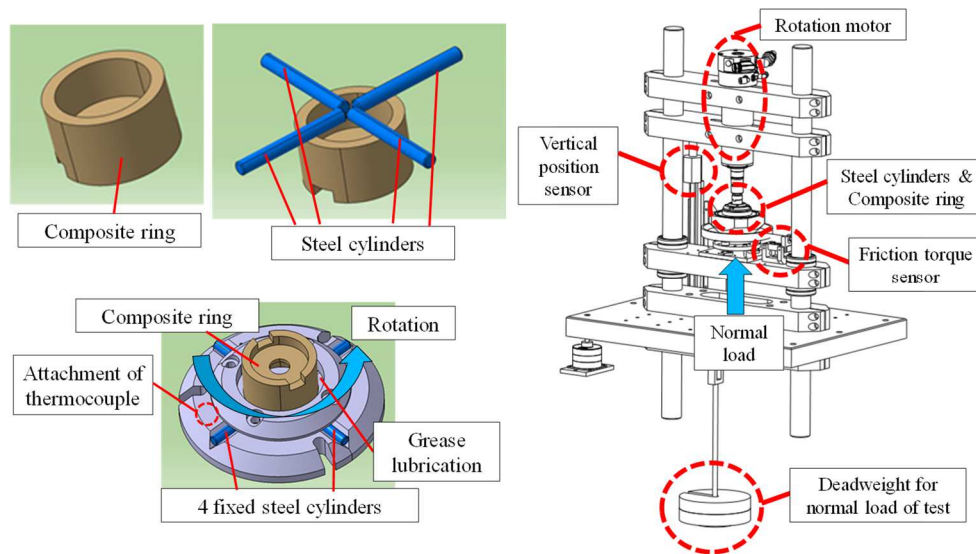


Fig. 2 Schematic view of test specimens and sliding test setup.

Table 4 Test conditions for sliding tests.

Steel cylinders (x4)	Diameter	3.5 mm		
	Length	30 mm		
	Material	Carbon steel with 0.45% of carbon		
	Young's modulus	205 GPa		
PA66 ring (JIS K 7218)	Outer diameter	25.6 mm		
	Inner diameter	20 mm		
	Height	12 mm		
Test conditions	Rotation speed	790 rpm		
	Mean sliding speed	1 m/s (Mean radius of the contact area: 11.4 mm)		
	Normal load	350 N		
	Hertzian maximum contact pressure	198 MPa (at 25 °C for GF-reinforced PA66) 136 MPa (at 25 °C for unreinforced PA66)		
	Test duration	88 min: intermittent process (10 s sliding and 1 s stopping)	25 min to 19.4 h: intermittent process (10 s sliding and 200 s stopping)	
	Total sliding cycles	61,500	1,000–43,000	
	Total sliding duration	80 min.	1.2– 55 min	
	Environment	25 °C	25–120 °C	

	temperature	
	Lubrication	Grease

2.5 Microscopy and surface analysis

Samples taken after the sliding tests were carefully washed using an ultrasonic bath in a heptane solvent (98%, Chimie-plus) for 20 min and ultrapure heptane (>99%, Chimie-plus) for 20 min to remove the attached grease and conduct the surface observations and analysis. The sliding surfaces after the tests were observed through SEM using an MIRA3 (TESCAN, Ltd.). Interferometry (Bruker, Ltd.) was used to observe the wear scar of the steel cylinders and evaluate the wear amount after the tests. An X-ray dispersive spectrometry (EDX) analysis was conducted to detect the chemical elements of a tribofilm under the boundary lubrication of the sliding surface of the steel cylinders and a PA66 ring. X-ray photoelectron spectroscopy (XPS) was conducted using a ULVAC-PHI Versa Probe II apparatus to detect the chemical states of the elements composing the tribofilm on the steel and PA66. The X-ray source is AlK_{α} operating at 1486.6 eV, and the size of the X-ray spot is 200 μm . A neutralizing electron gun was applied. The energy scale was calibrated using the C1s binding energy located at 284.8 eV. First, a wide range survey of 1,200 eV was conducted to identify all chemical elements with a pass energy of 187 eV. Next, a narrow range survey of each chemical element was conducted at a pass energy of 23 eV to identify the different chemical states, and a quantitative analysis was applied based on the curve fitting of each peak using Multipak software.

In addition, time-of-flight secondary ion mass spectrometry (ToF-SIMS) of the steel cylinders and PA66 ring after the tests was performed using a TOF-SIMS 5 (ION-TOF Co.) to detect the composition of the sliding surface. An area of $100 \times 100 \mu\text{m}^2$ was used for the spectroscopic analysis, and an area of $500 \times 500 \mu\text{m}^2$ was used for the chemical mapping. The depth of the analysis was lower than 10 Å (first monolayer). For the liquid metal ion gun (LMIG), Bi_3 was used as the source of the primary ions. Qualitative depth profiles on the steel cylinder were also investigated by repeating the low energy Cs^+ ion sputtering (500 eV) and conducting ToF-SIMS measurements.

3. Results and Discussion

3.1 Effects of adding zinc carboxylate to grease under test conditions with sliding heat generation using GF-reinforced PA66

Fig. 3 shows the evolutions of the friction coefficient, the temperature, and the vertical displacement under the test conditions for a stopping time of 1 s (after every 10 s of sliding) using a GF-reinforced PA66 composite and grease with or without zinc carboxylate (grease no. 1 and grease no. 2). In the first 10,000 cycles (when the temperature is below 60 °C), there is no effect of adding zinc carboxylate on the evolution of the friction coefficient and the temperature. However, the friction coefficient during the tests without zinc carboxylate increased after the temperature reached above 60 °C (the first 10,000 cycles), and a difference in the rate of

increase in temperature can be observed. The average friction coefficient during the sliding with zinc carboxylate is 0.059 ± 0.009 , which is 18.1% lower than the value without zinc carboxylate (0.072 ± 0.014). In addition, the rate of increase in the displacement is higher in the tests without zinc carboxylate, and a rapid increase in the displacement is observed at 45,000 and 52,000 cycles. Fig. 4 shows the height loss of the creep and wear of the composite ring after 61,500 cycles, which was estimated using the procedure described in Section 2.1. These results indicate that adding zinc carboxylate to grease decreases the creep of the composite because preventing the increase in temperature on the sliding surface related to a relatively lower friction coefficient prevents a degradation of mechanical properties and an increase in shear stress on the sliding surface. This confirms the friction reduction properties of this type of additive. Fig. 5 shows the observations of the sliding surface before and after the sliding tests with an optical microscope. As observed during the authors' previous study [42], the entire sliding surface of the composite ring undergoes peeling, and an exposure of the GF can be observed after the sliding tests. In addition, the sliding surface is expanded in both the inner and outer directions. The total area of the sliding surface is wider for the composite ring tested without zinc carboxylate, which is related to the large creep of the composite. This creep is caused by the decrease in the surface mechanical properties related to the damage by sliding, such as the scratching of PA66 or peeling off of fibers.

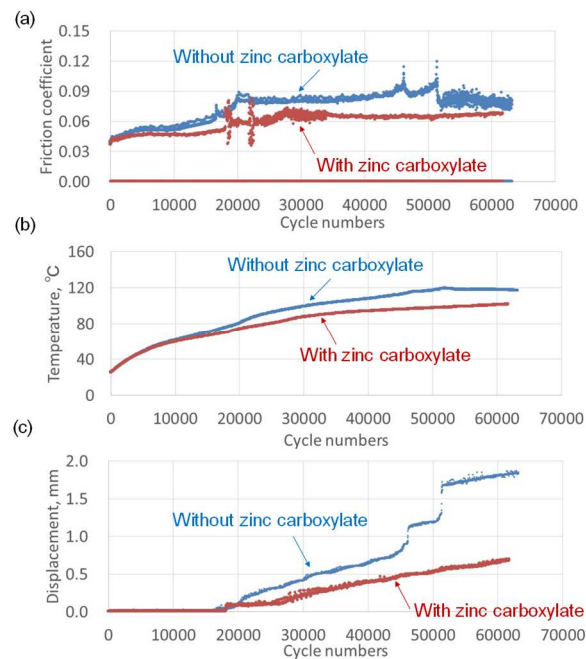


Fig. 3 Evolutions of (a) friction coefficient, (b) temperature, and (c) vertical displacement during the sliding test with GF-reinforced PA66 and grease with or without zinc carboxylate for a stopping time of 1 s.

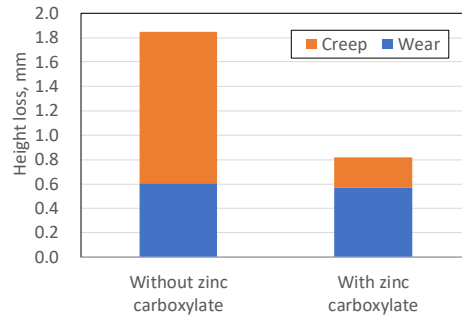


Fig. 4 Height loss of the creep and wear of the composite ring after 61,500 cycles.

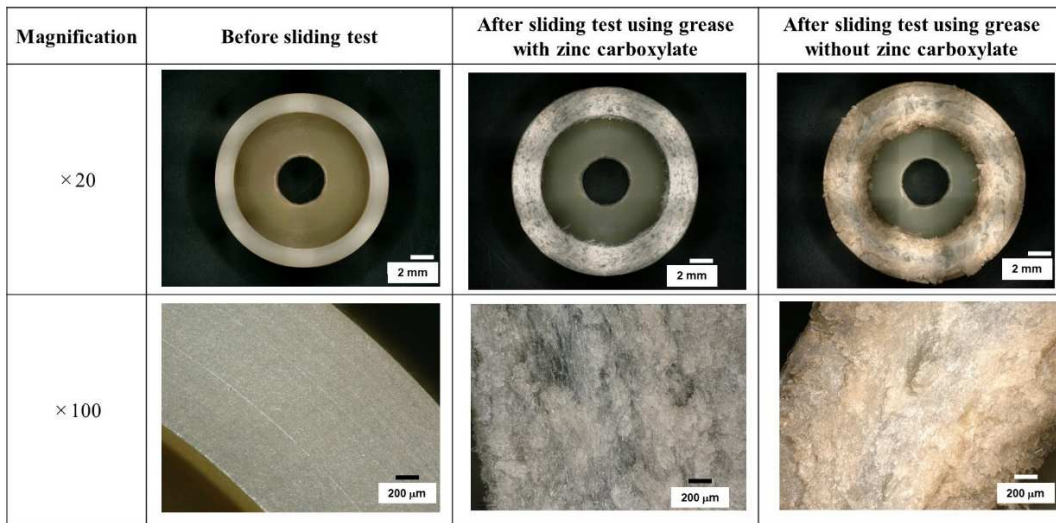


Fig. 5 Optical microscope observations of the sliding surface of the composite ring before and after the sliding tests.

3.2 Effects of adding zinc carboxylate to grease under test conditions at stable temperature using GF-reinforced PA66

Fig. 6 shows the height loss of the GF-reinforced PA66 composite (which is a summation of the wear and creep) after 42,000 cycles of the sliding tests for a stopping time of 200 s between each 10-s period of sliding (which allows us to control and maintain a given temperature for each test) at different temperatures, using grease with or without zinc carboxylate. When using grease without zinc carboxylate, the wear and creep increase with an increase in temperature from 25 °C to 80 °C. The wear then increases from 80 °C to 120 °C, and the creep presents almost the same value at 80 °C and 120 °C. In contrast, when using grease with zinc carboxylate, no increase in wear or creep at 80 °C is observed compared to those at room temperature, and increase at 100°C. In addition, no significant difference of wear and creep between 100 °C and 120 °C is observed.

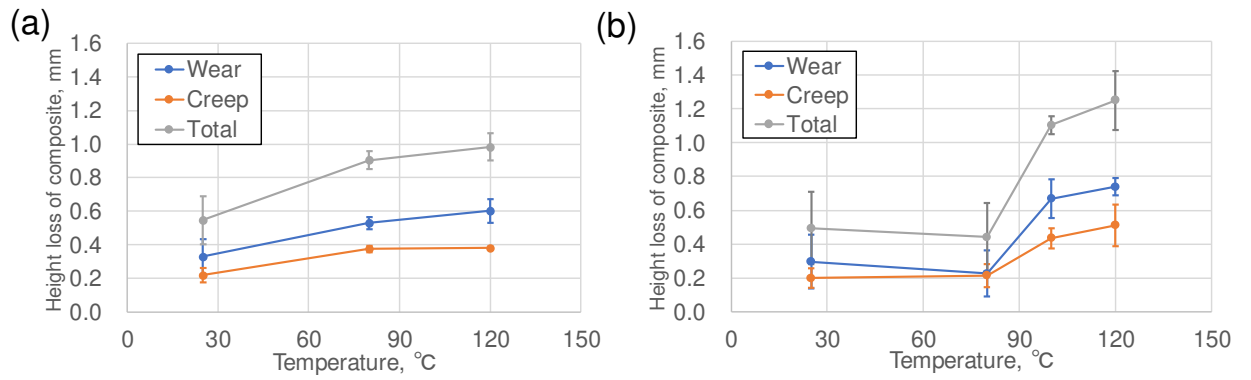


Fig. 6 Total height loss, wear height loss, and creep height loss of composite ring after 42,000 cycles during tests for a stopping time of 200 s

(a) without and (b) with zinc carboxylate in grease. Sliding tests were conducted for two times at each temperature.

Fig. 7 shows the sliding surface after the sliding tests. Worn surfaces of the composite ring are similar for the tests with or without zinc carboxylate, at both room temperature and 120 °C. At 80 °C, the width of the worn ring is smaller during the tests with zinc carboxylate added to the grease compared to tests without zinc carboxylate, confirming the beneficial effect of zinc carboxylate at this temperature level.

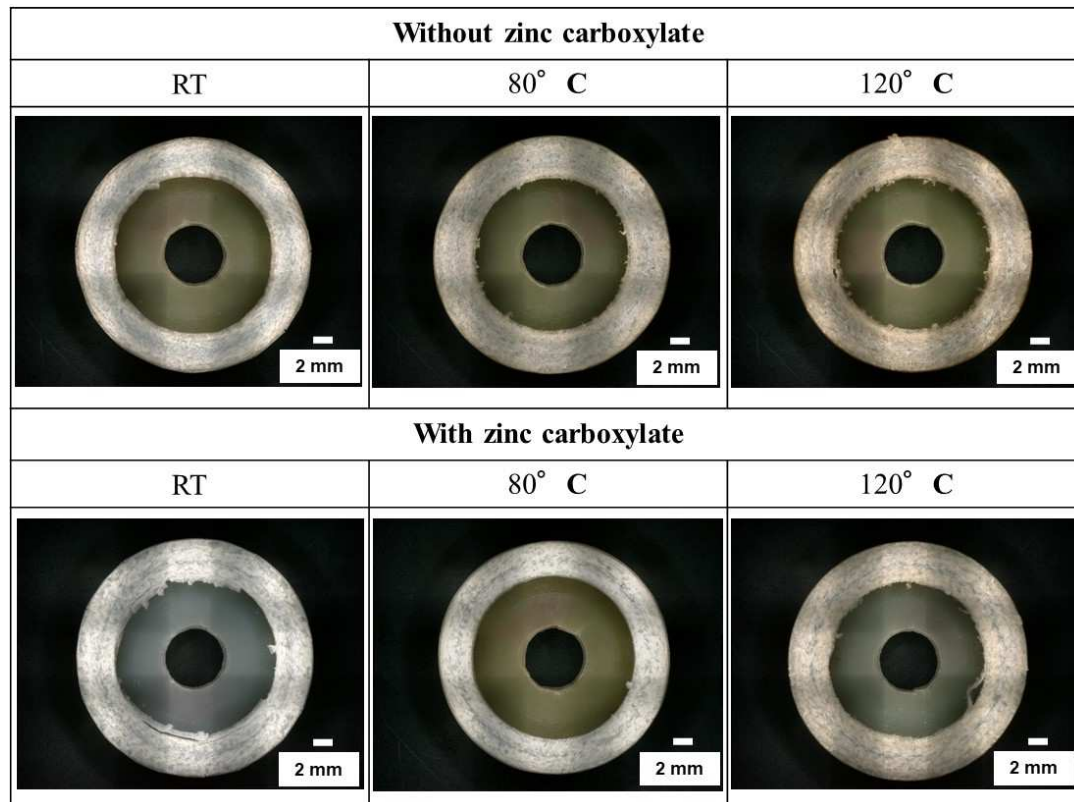


Fig. 7 Optical microscope observations on the sliding surface of the composite ring after sliding tests at room temperature, and at 80 °C and 120 °C, with or without zinc carboxylate applied to the grease.

Fig. 8 shows a load-displacement curve of the measurement on the sliding surface of the new GF composite ring and unreinforced PA66 ring (before the sliding test) measured as a function of temperature. Fig. 9 shows the evolution with temperature of the Young's modulus, hardness, and absolute creep displacement during the creep phase of the micro-indentation test (maximum normal load of 500 mN for GF composite and 250 mN for unreinforced PA66 maintained during a 10-s period). As expected, when the temperature is increased, the hardness and Young's modulus both decrease and the creep increases. In addition, the values of the hardness and Young's modulus of the GF composite are higher than those of the unreinforced PA66.

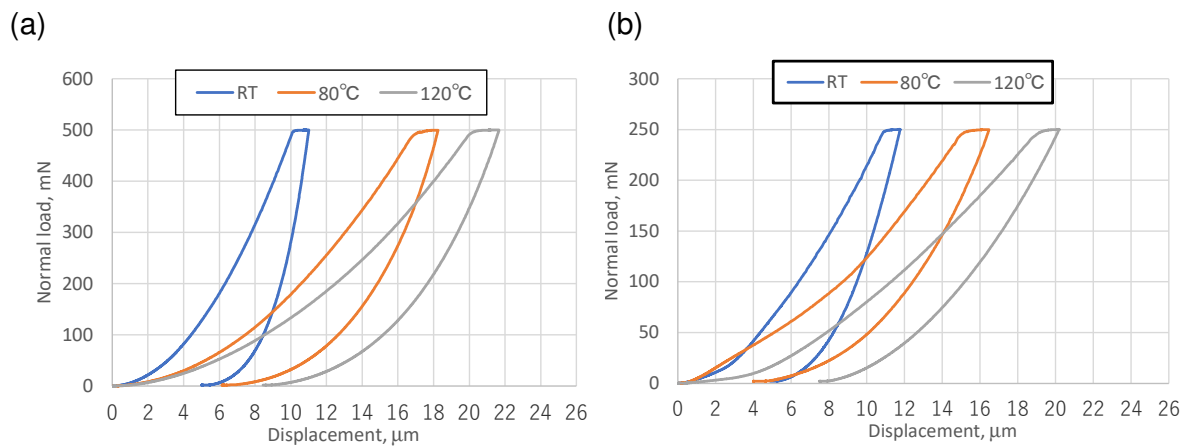


Fig. 8 Load–displacement curve of the measurement with the micro indentation at different temperatures.

(a) GF-reinforced PA66 composite; (b) unreinforced PA66.

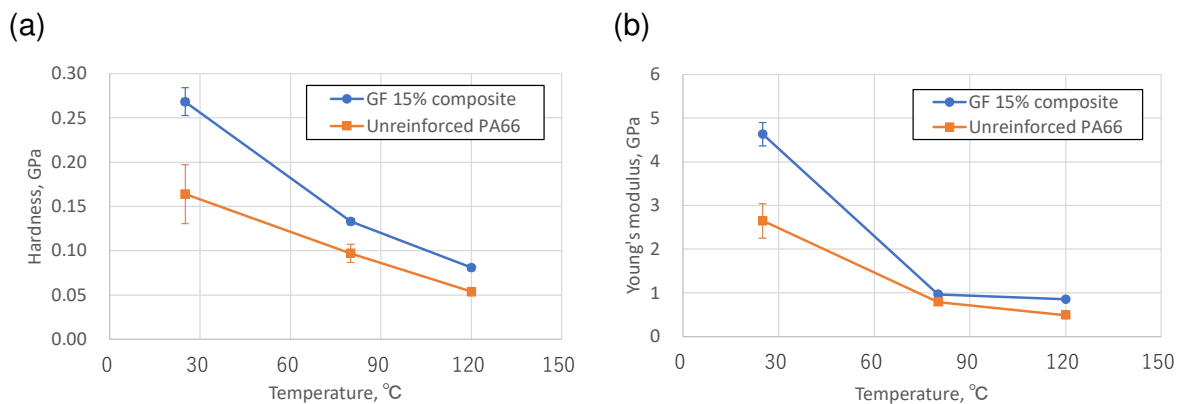


Fig. 9 (a) Hardness and (b) Young's modulus on the sliding surface of the GF-reinforced PA66 composite and unreinforced PA66 at different temperatures Measurement was conducted for three times at each temperature.

Fig. 10 shows the relationship between the hardness/Young's modulus of the GF composite surface and the wear height loss/creep height loss of the composite using grease with or without zinc carboxylate for different values of temperature. Fig. 10 shows that, without zinc carboxylate, good correlations occur between the hardness and wear height loss, and between the Young's modulus and creep height loss. Therefore, the wear and creep of the composite under test conditions using grease without zinc carboxylate can be explained based on the evolution of the elasto-visco-plastic mechanical properties of the composite as a function of temperature. However, no typical correlations were observed in the results with zinc carboxylate, leading to the conclusion

that the addition of the zinc carboxylate to grease has an impact on the tribological properties (through tribochemistry).

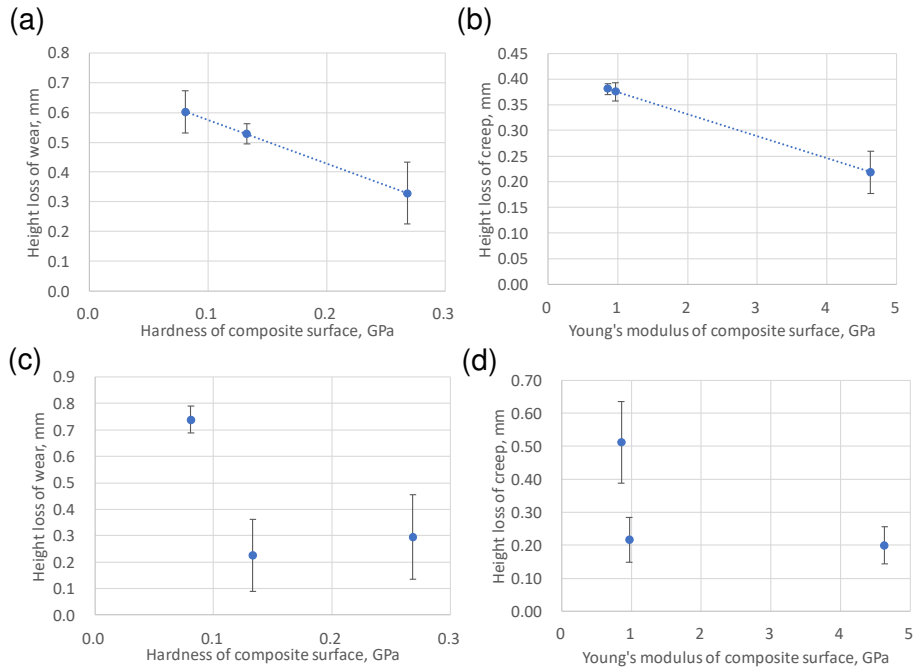


Fig. 10 Relationships between (a) the hardness of the composite and the wear height loss of the composite ring;(b) the Young's modulus of the composite and the creep height loss of the composite ring; ((a) and (b) without zinc carboxylate in grease);(c) the hardness of the composite and wear height loss of the composite ring; and (d) the Young's modulus of the composite and the creep height loss of the composite ring ((c) and (d) with zinc carboxylate in grease)

Fig. 11 shows the evolutions of the friction coefficient and the vertical displacement at room temperature under grease lubrication with or without zinc carboxylate. No differences in the friction coefficient and displacement can be observed, and the increase in the friction coefficient and the vertical displacement is observed after 10,000 cycles in both greases. This increase is related to the damage on the composite surface (peeling off of fibers and scratching of PA66) which induces the increase in the friction coefficient and sudden creep (plastic deformation), as presented in the authors' previous study [42]. Thus, the addition of zinc carboxylate to grease has no influence on the tribological properties at room temperature, confirming the results shown in Figs. 6 (a) and (b) for the tests conducted at room temperature.

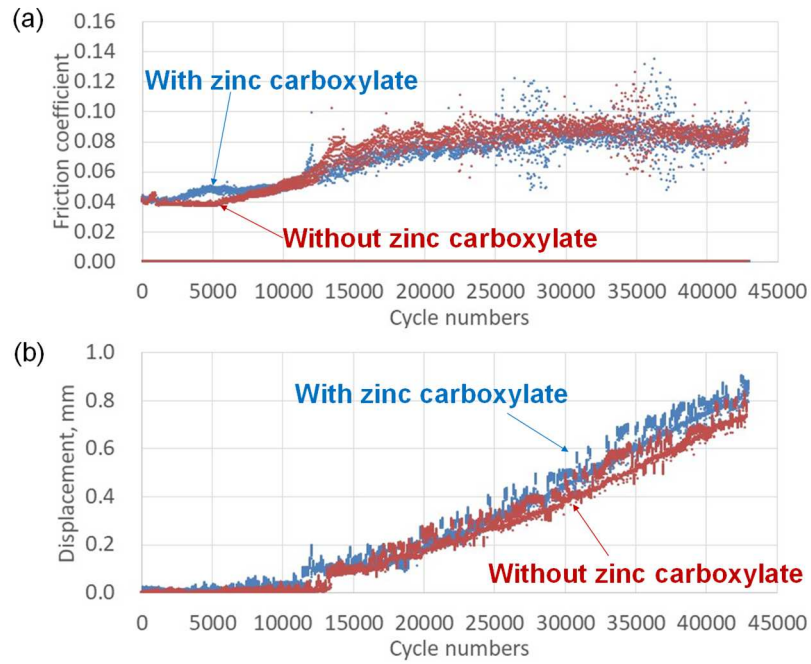


Fig. 11 Evolutions of (a) friction coefficient and (b) vertical displacement at room temperature using grease with or without zinc carboxylate.

Fig. 12 shows the evolutions of the friction coefficient and the displacement at 80 °C. Significant differences in both the friction coefficient and displacement can be observed for tests with or without zinc carboxylate in grease. Using grease with zinc carboxylate, the friction coefficient decreases during the initial stage of the sliding, and sudden increases in the friction coefficient and displacement are observed at larger numbers of cycles ($27,500 \pm 5,000$ cycles) than without zinc carboxylate (11,000 cycles). The average value of the friction coefficient during the initial 5,000 cycles when using grease without zinc carboxylate is 0.045, and is 0.037 with zinc carboxylate (a decrease of 22.0%). After 43,000 cycles, the displacement is 0.472 ± 0.092 mm for tests with zinc carboxylate, compared to 0.989 ± 0.004 mm for tests without zinc carboxylate, confirming the results shown in Figs. 6 (a) and (b) at 80 °C.

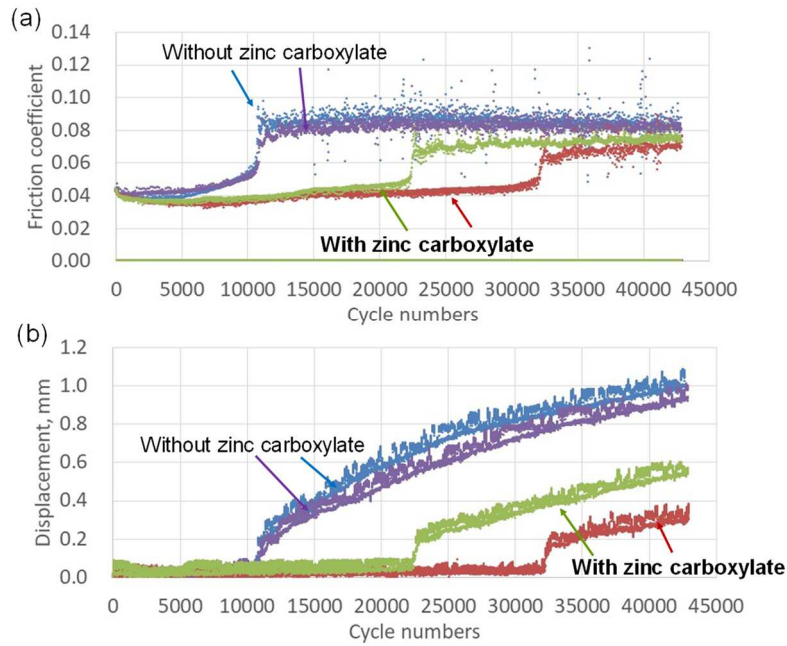


Fig. 12 Evolutions of (a) friction coefficient and (b) vertical displacement at 80 °C using grease with or without zinc carboxylate.

Fig. 13 shows the evolutions of the friction coefficient and the displacement at 120 °C. The effect of the decrease in the friction coefficient is observed during both the initial phase of the sliding and after the increase in friction. However, no beneficial effect on the displacement is observed. We can even conclude that, at 120 °C, displacement is higher when zinc carboxylate is added to grease, confirming the results shown in Figs. 6 (a) and (b) at 120 °C. Given these results, it was confirmed that the effects of the addition of zinc carboxylate on grease differ at each temperature.

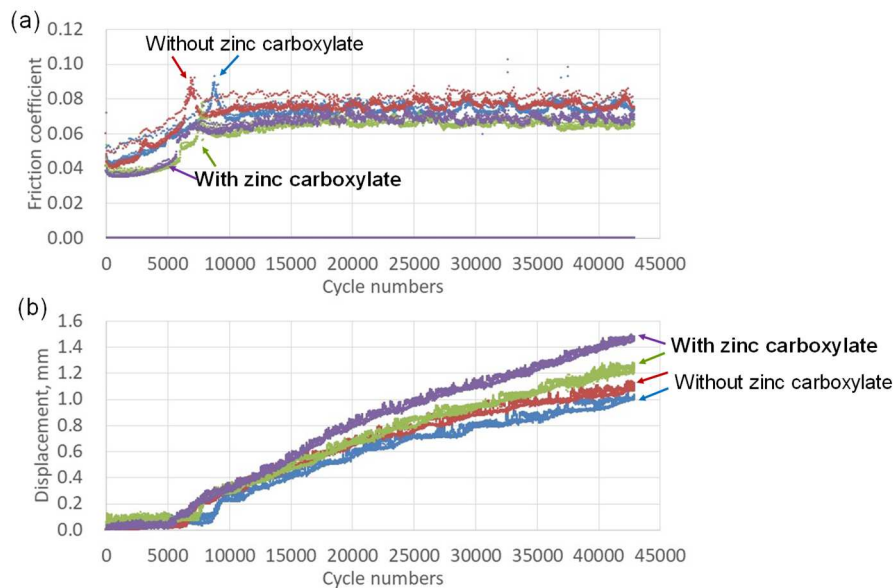


Fig. 13 Evolutions of (a) friction coefficient and (b) vertical displacement at 120 °C using grease with or without zinc carboxylate.

In addition, Fig. 14 shows the contributions of the increase in temperature and the addition of zinc carboxylate to grease on the increase in the wear and creep height losses of the composite. Negative values represent improvements in the tribological properties (i.e., the decrease in wear and creep), and positive values represent the deterioration in the tribological properties (i.e., the increase in wear and creep), when considering that the base value is the result at room temperature using grease without zinc carboxylate. The results indicate that the addition of zinc carboxylate to grease has a weak impact on the wear and creep resistance at room temperature. The positive effect of the addition of zinc carboxylate on the improvement of the wear and creep resistance is greater than the negative effects of the increase in temperature at 80 °C. However, improvements in the wear and creep resistance by the addition of zinc carboxylate were not observed at 120 °C.

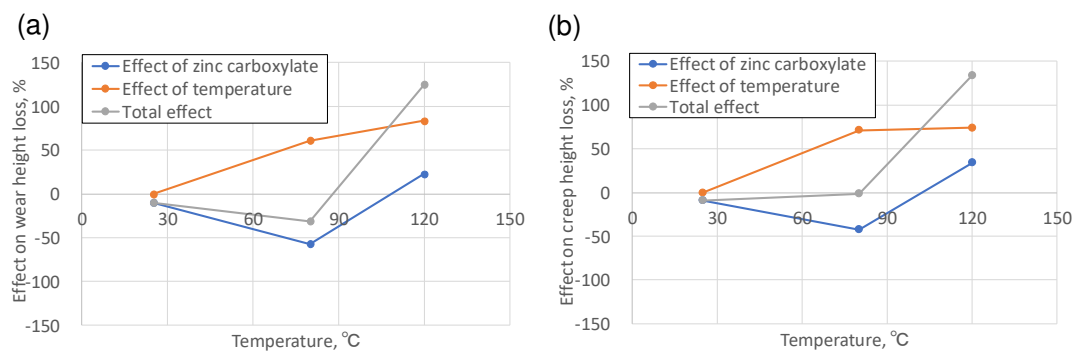


Fig. 14 Contribution of the increase in temperature and the addition of zinc carboxylate to grease toward the (a) wear and (b) creep height losses.

*The base value indicates the results at room temperature using grease without zinc carboxylate.

Fig. 15 shows the wear volume of the steel counterpart (total wear amount of four cylinders) at each temperature using grease with or without zinc carboxylate, and Fig. 16 shows the optical microscope observation of the steel cylinder after sliding tests at different temperatures. The wear of the steel cylinders, which is considered to be 2-body abrasive wear observed in the sliding direction related to the presence of GFs, increases globally with an increase in the temperature. By contrast, the effect of the decrease in the wear amounts of the steel cylinders is observed by the addition of zinc carboxylate at 80 °C.

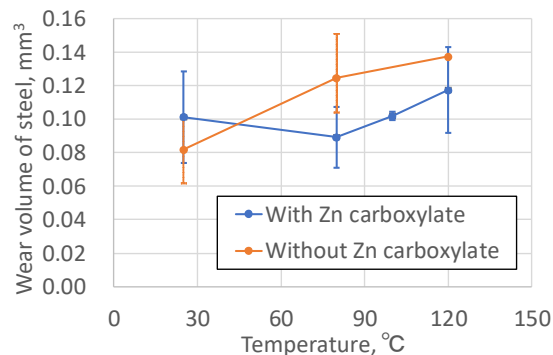


Fig. 15 Wear volume of steel cylinders at each temperature using grease with or without zinc carboxylate (average value of two measurements).

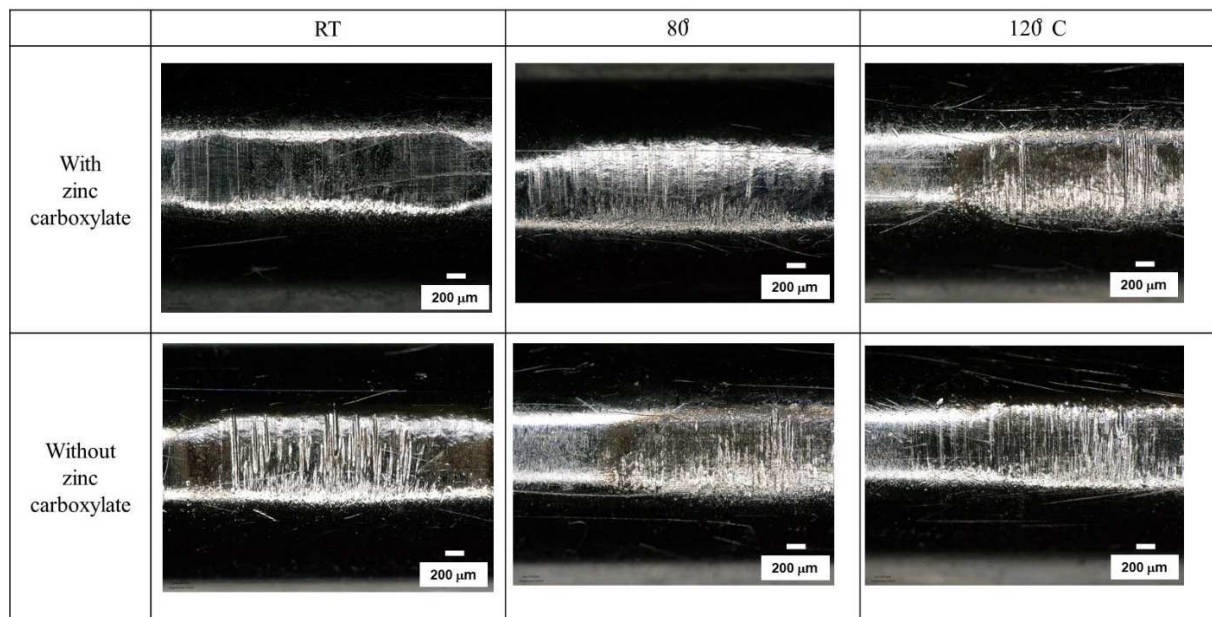


Fig. 16 Optical microscope observation of steel surface after sliding tests at different temperatures.

The results presented in this section confirm that the addition of zinc carboxylate plays a role in the tribological properties of the contact under investigation, and that this effect depends on the temperature. Because we can expect this effect to be related to the tribochemical reactions, it may be interesting to analyze the surface chemistry of the wear scars at 80 °C (where the beneficial effect is the most important), which is the objective described in the next section.

3.3 Identification of the tribofilm on the surface of steel and composite at 80 °C

To clarify the improvements on the tribological properties through the addition of zinc carboxylate to grease at 80 °C, sliding surfaces of steel cylinders and a GF-reinforced PA66 composite after 13,000 cycles of the sliding test for a stopping time of 200 s (before the sudden increase in the vertical displacement) were analyzed.

Fig. 17 shows SEM images of the sliding surface of a steel cylinder. Numerous dark heterogeneous patches from the submicron level to 20 μm in size can be seen on the sliding surface after the test. The results of the SEM-EDX point analysis of the dark patches presented in Fig. 18 indicate that the proportion of Fe decreases in the patch area compared to the no patch area, and that these patches are composed of the chemical elements of hydrocarbon (C, O) and small amounts of elements related to the additives of grease (Zn, S). These patches were not removed after an additional washing with an ultrasonic using heptane solvent for 20 min. after the first SEM-EDX analysis for 20 min., and they remained completely at a fixed location. Therefore, these patches were strongly adhered to the sliding surface of the steel cylinders.

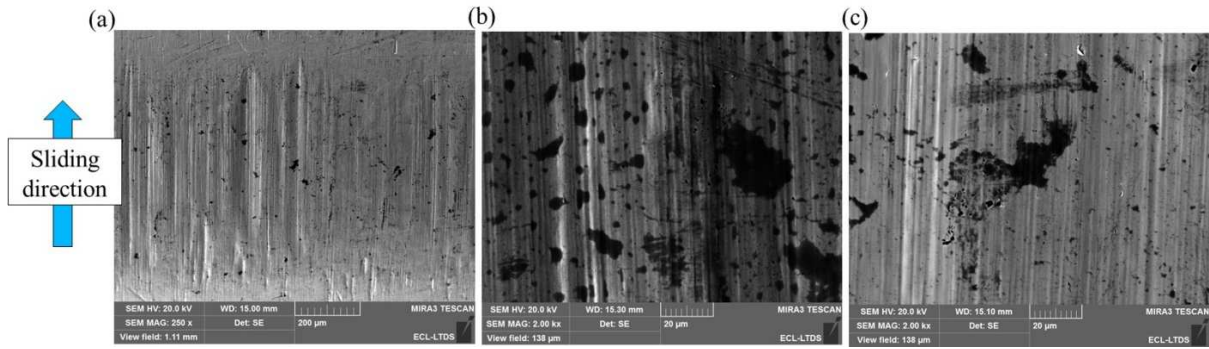


Fig. 17 SEM images on the sliding surface of a steel cylinder after 13,000 cycles. (a) at a magnification of $\times 300$: (b) and (c) at a magnification of $\times 2000$.

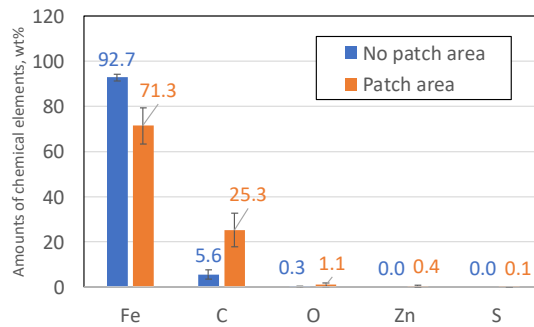


Fig. 18 Amounts of each chemical element measured using a point analysis of SEM-EDX (average value of five measurements).

Fig. 19 shows the SEM images of a new steel cylinder (without sliding tests) and a cylinder heated with grease at $80\text{ }^{\circ}\text{C}$ for 6 h in contact with a composite ring at a normal load of 350 N (the same temperature, normal load, and duration as the sliding tests over 13,000 cycles, but without sliding) after the same washing process. Patches containing the same types of chemical elements (C, O) are also observed on the surface of the cylinder without sliding (Fig. 19 b). Therefore, these patches after sliding for 13,000 cycles would be an adsorbed film related to heating with grease or mixture of an adsorbed film and a tribofilm formed during the sliding tests as a consequence of the tribochemical reactions between the additives in the grease and the material surfaces under contact pressure, shear, and temperature. To identify the detailed chemical compositions of these patches and confirm whether these patches are the tribofilm or not, we conducted additional chemical analyses.

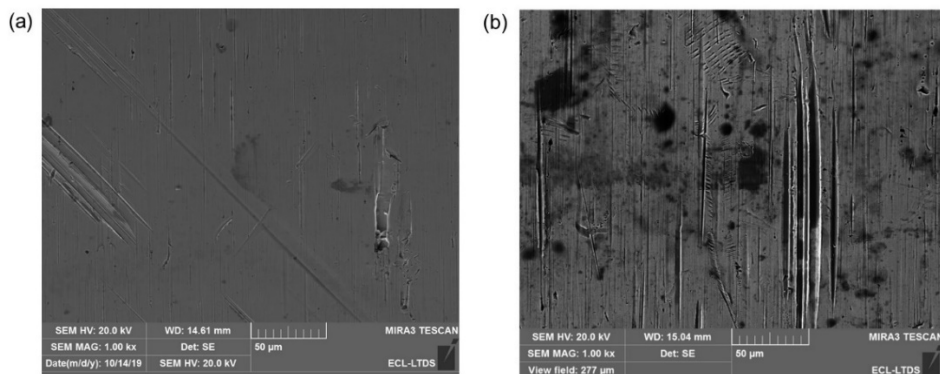


Fig. 19 SEM images of (a) new steel cylinder (without sliding tests) and

(b) cylinder heated with grease at 80 °C for 6 h in contact with a composite ring without sliding

The XPS analysis results did not identify the composition of the patches (film) on the surface of the steel cylinder, which is composed of hydrocarbon, because it was not possible to distinguish explicitly the adventitious carbon originating from the contamination in atmosphere and the hydrocarbon on the tribofilm. Therefore, a ToF-SIMS analysis was conducted to identify the composition of the hydrocarbon film, including the surface of the new steel cylinder, the cylinder after 13,000 cycles of the sliding test with no wear area (with grease contact for 6 h at 80 °C), and the cylinder in wear area, as presented in Fig. 20.

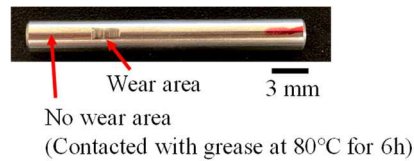


Fig. 20 ToF-SIMS analysis areas of the steel cylinder (observed using a microscope).

Fig. 21 shows the relative intensities of the detected carboxylates ions in each analyzed area, which were obtained based on the normalization of the intensity of FeO_2^- . Fig. 22 shows the chemical mapping of stearic and palmitic ions on the steel cylinder after the sliding test in the no wear and wear areas (the decrease in the concentration of ions at the top and bottom of all images is due to the curvature of the steel cylinder). Six different types of carboxylates were detected from all analyzed surfaces, with palmitic and stearic ions having the highest concentrations. Palmitic and stearic ions particularly increase in the no wear area as compared to the surface of the new cylinder (without a sliding test). It is then considered that different types of carboxylates coming from zinc carboxylates additive added to the grease were adsorbed into the steel surface by heating at 80 °C. Furthermore, the intensities of the carboxylates ions on the wear surface are greater than on the no wear area. This indicates that the formation of the tribofilm was accelerated by the energy induced by the sliding (i.e., the pressure, shear, and heat), in addition to the simply adsorbed film. Chemical mapping images indicate that the intensities of the stearic or palmitic ions are higher in all areas of the sliding surface than on the surface without sliding. In addition, the same types of carboxylates are detected even on the surface of the new cylinder after the same washing process using an ultrasonic and organic solvent. Some of these carboxylates are thought to be derived from the oil used during the machining process of the steel cylinders, or rust-preventive oil used during the preservation of the steel cylinders.

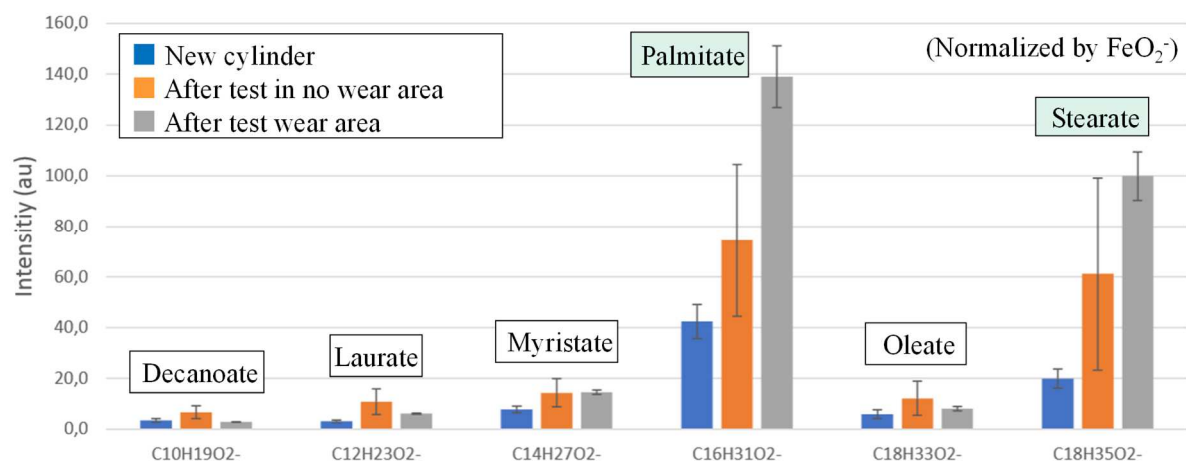


Fig. 21 Relative intensities of carboxylates in each analyzed area on the steel surface measured using ToF-SIMS. (average value of three different analyses).

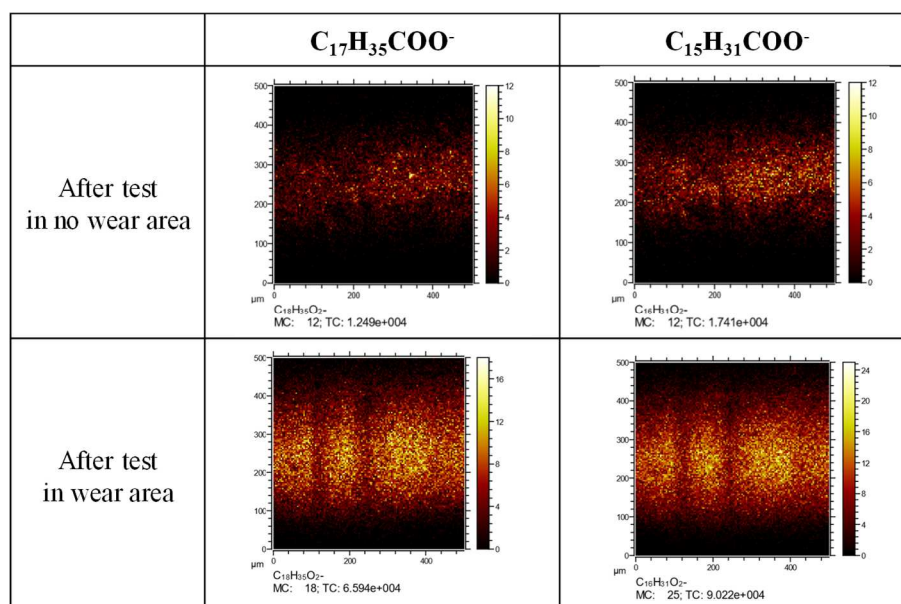


Fig. 22 Chemical mapping of stearic and palmitic ions on the steel cylinders analyzed using ToF-SIMS.

Furthermore, a depth profile analysis was conducted to investigate the presence of the film from the outermost surface to the core of the substrate. Fig. 23 shows the depth profile of the steel cylinder after 13,000 cycles of the sliding test in the no wear area (in contact with the grease at 80 °C for 6 h) and the wear area. The intensities are normalized by the iron bulk signal at the end of the profiles. In both areas, an iron oxide layer is observed on the steel surface, and the depth profile is similar. However, much larger amounts of carboxylates (stearic or palmitic ions) are present on the surface of the wear area compared to the no wear area. Both carboxylates and iron oxide (Fe_2O_4) decrease gradually with an increase in the sputter time. Therefore, it is believed that a non-uniform carboxylates-based tribofilm is present on the iron oxide layer. Fig. 24 shows 3D images of the repartition of stearic and palmitic ions (observed area of $80 \mu m \times 80 \mu m$, where the depth of scale of the 3D images is unknown, but is extremely small compared to $80 \mu m$) and 2D images of stearic ions

observed from the top surface in both the no wear and wear areas. In the wear area, stearic and palmitic ions are heterogeneously distributed, and also exist in the form of spots (indicating a high local concentration of carboxylates) on the sliding surface. The lateral size of these spots is approximately 5–20 μm , i.e., the same size as the dark patches observed using SEM. The depth of these spots cannot be precisely measured, but we may expect that it is more at the nano-scale than at the micro-scale (considering the measurement depth of ToF-SIMS). Therefore, these spots are considered to be formed from softened carboxylates that form the iron carboxylates on the steel surface [34].

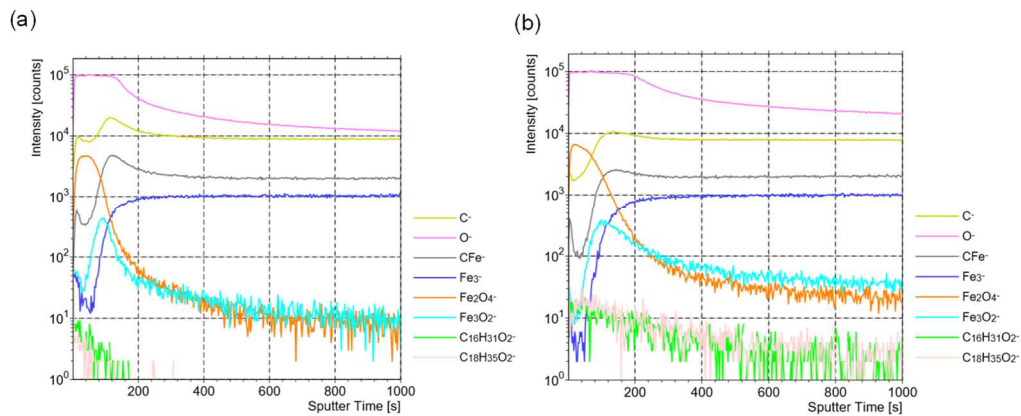


Fig. 23 Depth profile of ToF-SIMS analysis on the steel cylinder: (a) no wear and (b) wear areas.

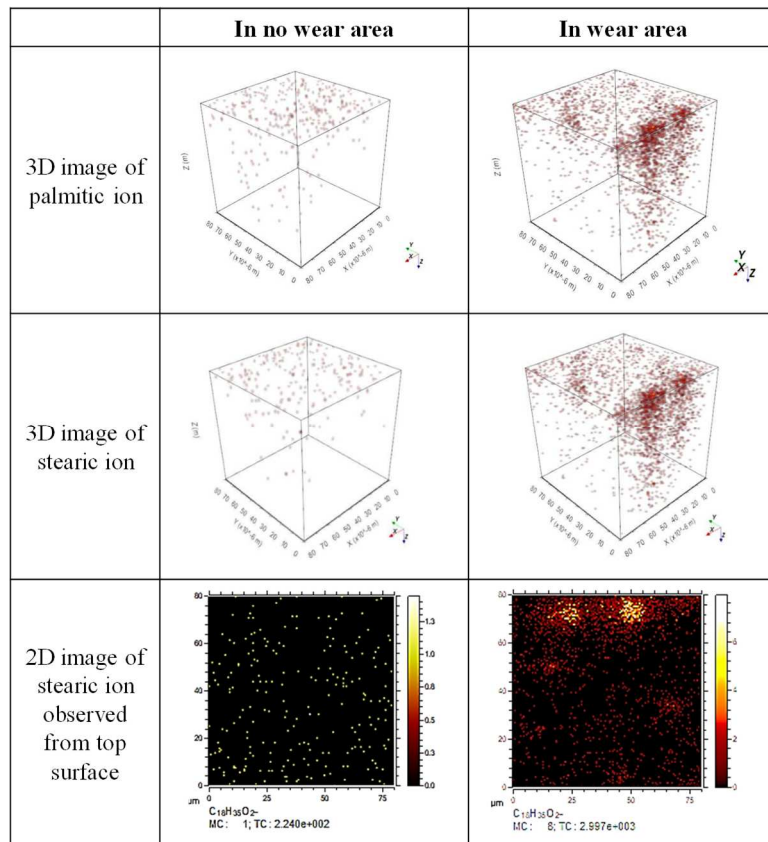


Fig. 24 3D images of stearic and palmitic ions (observed area of $80 \mu\text{m} \times 80 \mu\text{m}$) and 2D images of stearic ions observed from the top surface in the no wear area and the wear area analyzed using ToF-SIMS.

Fig. 25 shows the relative intensity of Zn^+ (originating from zinc carboxylate in the grease) on the surface of each steel cylinder normalized based on the signal of Fe^+ and analyzed using ToF-SIMS. The number of zinc ions is higher on the cylinder surface after 13,000 cycles of the sliding test in the no wear area than in the new cylinder without sliding. However, the number of zinc ions in the cylinder in the wear area is lower than that in the no wear area. In addition, Fig. 26 shows the chemical mapping images of Zn^+ , SO_3^- , CSN^- , and CNO^- (the last three ions are considered to have originated from the sulfur-type anti-oxidation agent or diurea thickener in the grease, and the agent related to the base oil was not observed) on the surface of the steel cylinder analyzed using ToF-SIMS. The intensities of these peaks on the surface of the no wear area are higher than those in the wear area. This tendency differs from the analysis results of the carboxylates (palmitate or stearate).

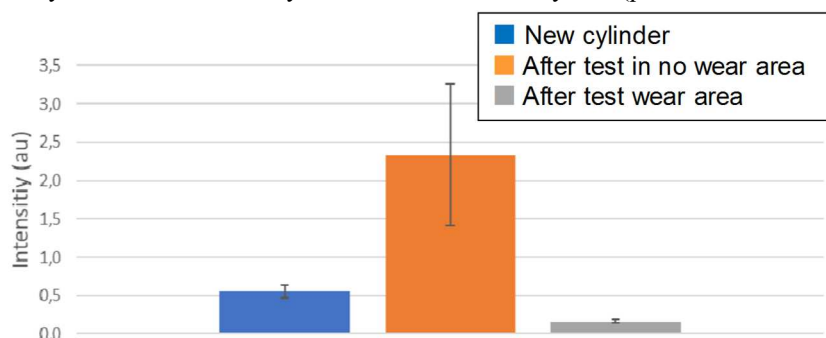


Fig. 25 Relative intensity of Zn^+ on the surface of each steel cylinder normalized by the Fe^+ signal through a ToF-SIMS analysis (average value of three different analyses).

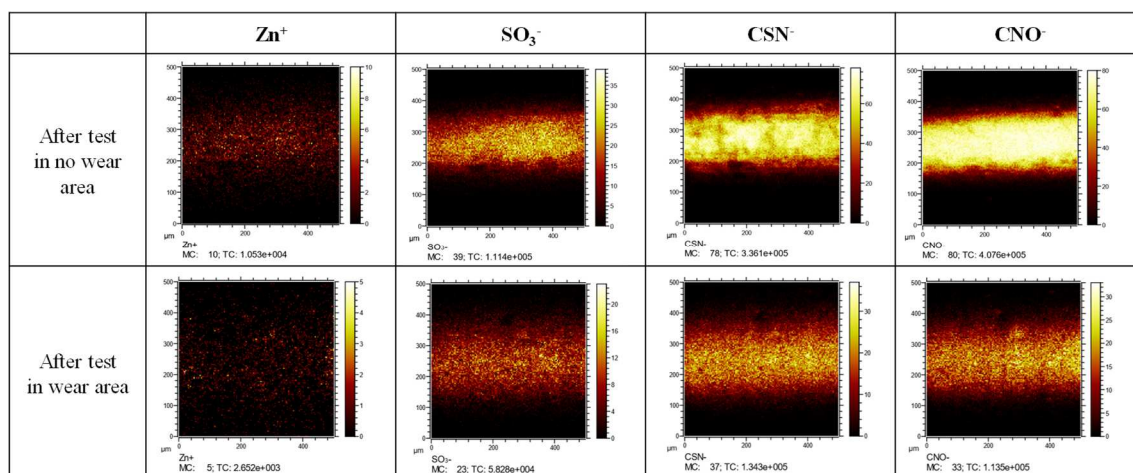


Fig. 26 Chemical mapping of Zn^+ , SO_3^- , CSN^- , and CNO^- based on a ToF-SIMS analysis on the surface of the steel cylinder in the no wear area or the wear area.

The chemical composition on the surface of the GF-reinforced PA66 ring was analyzed to clarify the chemical reaction on the composite. Fig. 27 shows the evolution of the amounts of Zn and S on the sliding surface of the composite after different numbers of cycles of the sliding tests at 80 °C as measured using SEM-EDX, presenting the evolutions of the vertical displacement and the friction coefficient of the sliding test

described in Section 3.2. Although Zn and S were not detected from the surface of the composite ring after 1,000 cycles, the amounts of Zn and S increase after 5,000 cycles until the sudden increase of the vertical displacement, and decrease at 42,000 cycles. Fig. 28 shows the SEM and EDX images of Si (related to the GF), and Zn and S after 13,000 cycles of the sliding test at 80 °C. There is a tendency for Zn and S to exist at the same location of the composite ring.

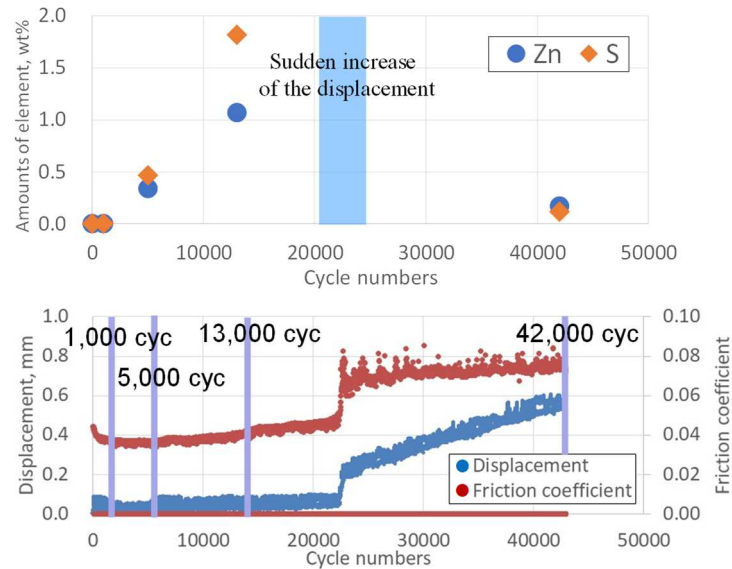


Fig. 27 Evolution of the amounts of Zn and S on the sliding surface of the composite after different numbers of cycles of the sliding test at 80 °C as measured using SEM-EDX.

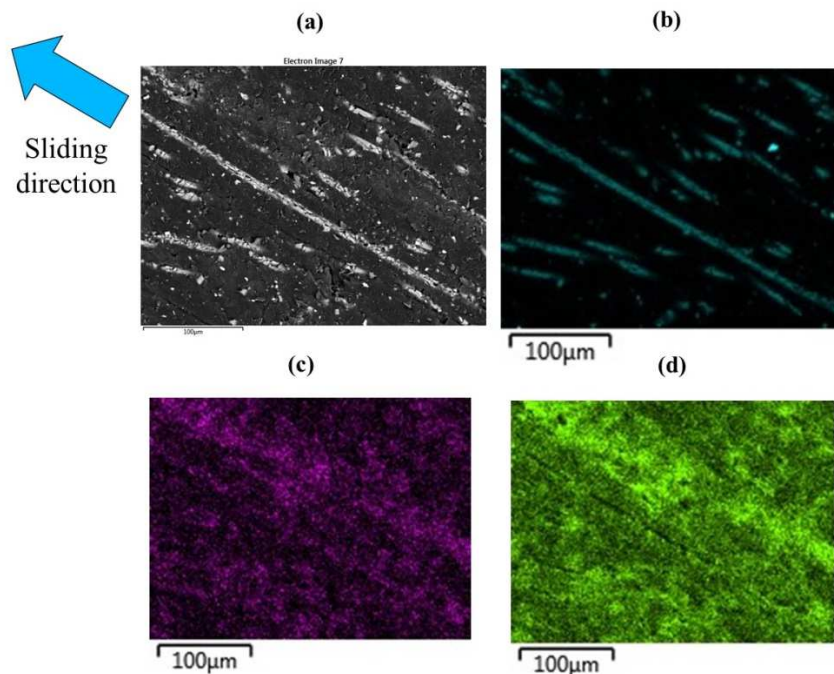


Fig. 28 SEM and EDX images of composite surface after 13,000 cycles of the sliding test at 80 °C;
 (a) SEM image and EDX images of (b) Si, (c) Zn, and (d) S.

To identify the chemical states of Zn and S, an XPS analysis of the sliding surface of GF-reinforced PA66 composite after 13,000 cycles of the sliding test at 80 °C was carried out. Four different areas of the sliding surface (the inner area, two different center areas, and the outer area) were analyzed, along with the surface of the new composite ring as a baseline. Fig. 29 presents the obtained chart of XPS analysis in wide range analysis, and narrow range analysis of S and Zn. These results show that the peaks of S_{2p} and Zn_{2p3} are detected only on the surface after the tests in the four analyzed areas. The position of the S_{2p} peak indicates the presence of a sulfide and agrees well with the binding energies measured in ZnS [48, 49]. The measured binding energy for Zn of 1021.6 eV can correspond to both ZnO or ZnS [48, 49]; however, because no metal oxide contribution is found in the O1s region, it is probable that the signal in Zn_{2p} is related to ZnS almost entirely. In addition, the fitting data of these peaks listed in Table 5 indicate that the atomic ratio of S_{2p} and Zn_{2p3} is approximately the same, and that the atomic ratio of S_{2p} and Zn_{2p3} is near 1. Therefore, the formation of a reactive ZnS tribofilm by the reaction of zinc carboxylate and a sulfur-type anti-oxidation agent induced by sliding was identified.

In addition, to investigate the presence or not of a carboxylates film on the surface of the GF-reinforced PA66 composite ring, a ToF-SIMS analysis of the composite surface was also conducted. However, no peaks of carboxylates (palmitic or stearic ions) were detected from the surface of the new composite ring (without a sliding test), the composite ring in which a 350 N normal load was applied for 6 h under grease lubrication at 80 °C, or the composite ring after 13,000 cycles of the sliding test at 80 °C, contrary to the results obtained for the surface of the steel cylinder after the same number of cycles. This result indicates that carboxylates preferentially adhere to the surface of the steel and do not adhere to the surface of GF-reinforced PA66.

To investigate the location of the ZnS tribofilm on the surface of the composite, a SEM-EDX point analysis was conducted on the PA66 and GF surfaces using the same composite ring after 13,000 cycles of the sliding test at 80 °C. Fig. 30 shows the amounts of each chemical element on the surfaces of the PA66 and GF (composed of Si, Ca, Al, and Mg). The average values of the measurement at five different locations are shown. The results indicate that a ZnS tribofilm is only present on the surface of the PA66, and no ZnS tribofilm was identified on the surface of the GF, the reason for which is related to the difference in the contact pressure in each area. The hardness of the GF (5.8 GPa measured based on the nano indentation) is much higher than the hardness of the PA66 (0.2 GPa measured based on the micro indentation). Therefore, the partial contact pressure between the GF and steel increases, and if formed, the ZnS tribofilm on the GF is considered to be easily peeled off by the sliding.

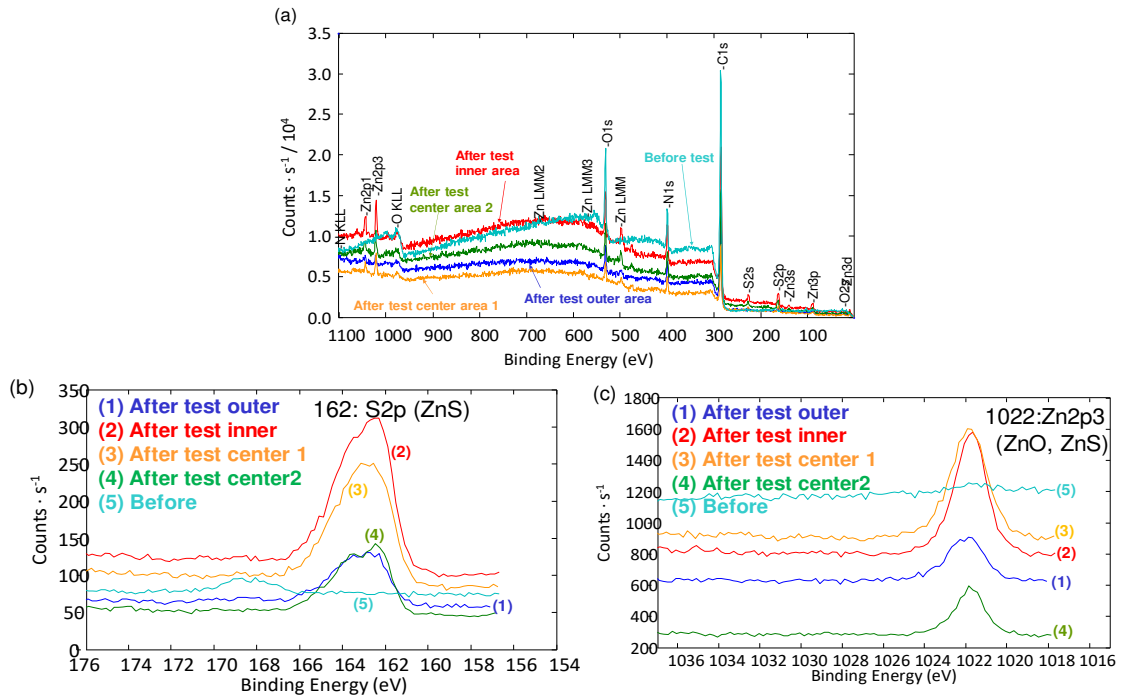


Fig. 29 Results of XPS analysis of composite surface before/after the sliding tests for 13,000 cycles at 80 °C using the grease containing zinc carboxylate and sulfur-type anti-oxidation agent:
 (a) wide scanning; and (b) narrow scanning of S_{2p} and (c) narrow scanning of Zn_{2p₃}

Table 5 Amounts of each chemical state estimated based on the curve fitting of the XPS analysis results.

	162 eV S _{2p}	1022 eV Zn _{2p₃}	Ratio of S _{2p} /Zn _{2p₃}
After test of outer area	0.9 at%	1.0 at%	0.9
After test of center area 1	1.7 at%	1.9 at%	0.9
After test of center area 2	1.7 at%	1.3 at%	1.3
After test of inner area	1.7 at%	1.5 at%	1.1
Before test	0.0 at%	0.1 at%	0.0

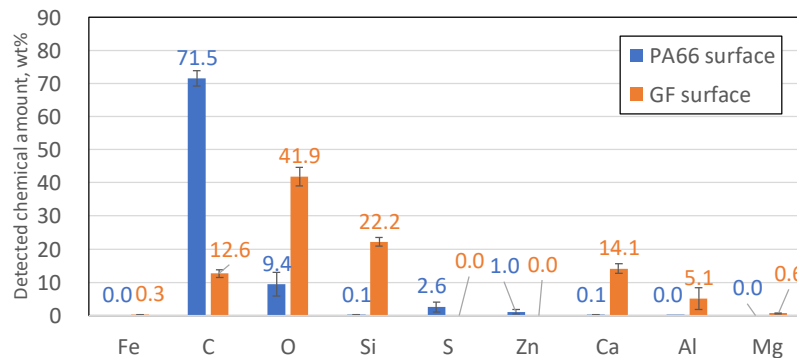


Fig. 30 Amounts of chemical element on the surface of PA66 and GF measured using SEM-EDX after 13,000

cycles of the sliding test at 80 °C using grease which contains zinc carboxylate and sulfur-type anti-oxidation agent (average value of five different measurement areas).

Fig. 31 shows sketches of the tribochemical reaction on the sliding surface of the composite and steel. For the sake of simplicity, the roughness of either counterbody (which is much larger than the sizes of the molecules) is not shown in these images. The carboxylates of zinc carboxylates additives bind to the iron of the steel surface to form what is called in literature a “soap” layer (iron carboxylates [34, 50]), and zinc goes to the polymer part of the composite and reacts with sulfur present in the anti-oxidation agent.

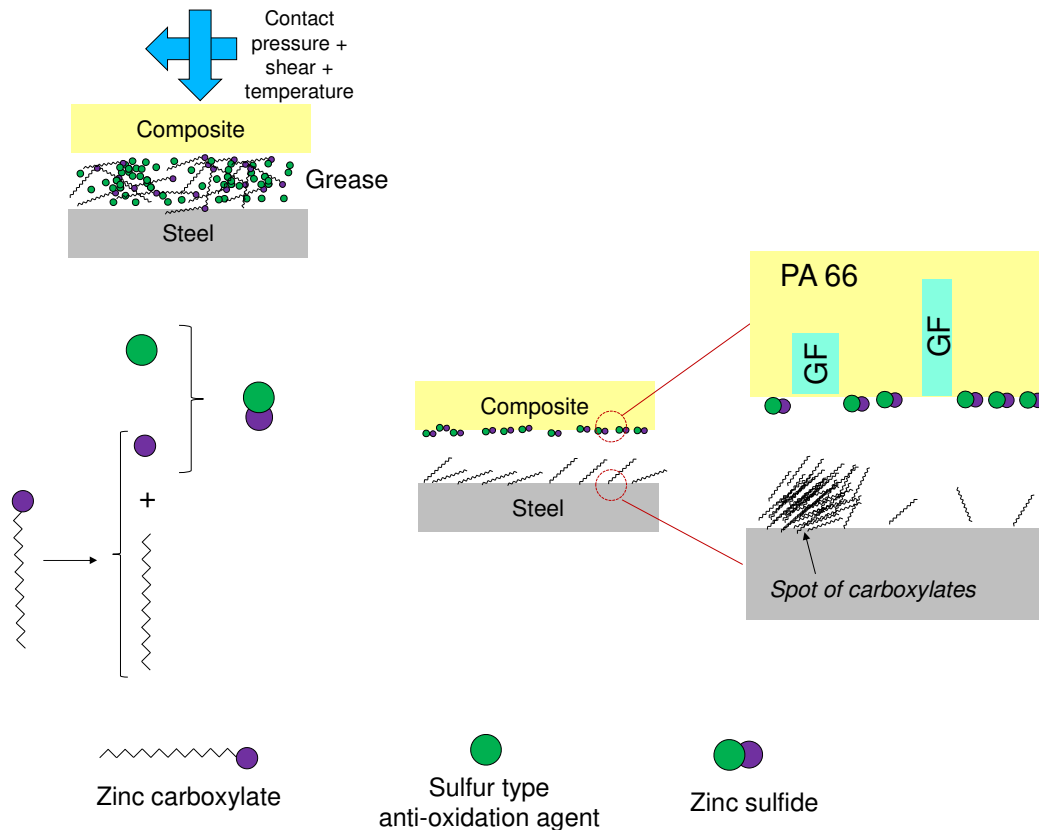


Fig. 31 Tribochemical reaction on the sliding surface. The lateral and depth scales are not respected in these images.

3.4 Contribution and roles of tribofilm on the tribological properties

To clarify the effects of the carboxylate tribofilm on the steel surface and the effects of the ZnS tribofilm on the PA66 surface on the improvement of the tribological properties, additional sliding tests were conducted at 80 °C using grease containing zinc carboxylate but not a sulfur-type anti-oxidation agent (grease no. 3), applying a stopping time of 200 s (allowing us to maintain a constant temperature), using GF-reinforced composite. Fig. 32 shows the evolutions of the friction coefficient and the vertical displacement, comparing the results of grease no. 1 and grease no. 2, as previously shown in Fig. 12. Using grease no. 3, the sudden increase in the friction coefficient and the vertical displacement appear much later than the results of grease no. 2 (without zinc carboxylate but with a sulfur-type anti-oxidation agent). By comparing the results with grease no.

3 and grease no. 1, we can conclude that, with zinc carboxylate present in the grease, the addition of a sulfur-type anti-oxidation agent allow a low-friction coefficient to be maintained for a greater number of cycles, leading to lower wear; however, this has no impact on the friction coefficient values before or after the sudden increase, indicating that the effects of the addition of zinc carboxylate on the improvement of the tribological properties is greater than the effect of the addition of a sulfur-type anti-oxidation agent. Consequently, we can conclude that a reduction in the friction induced by the creation of carboxylates patches on the steel cylinder is the main effect of the presence of additives in the grease, and on the tribological behavior of the contact.

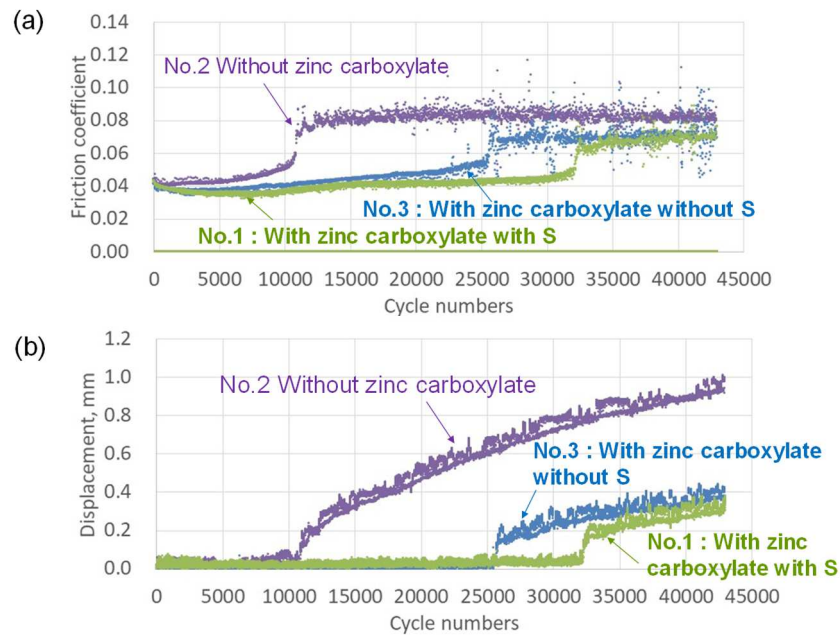


Fig. 32 Evolution of (a) friction coefficient and (b) displacement during the sliding test at 80 °C using grease 1, 2, and 3 and GF-reinforced composite.

Fig. 33 shows a narrow scan analysis of the XPS in the composite surface after 13,000 cycles of a sliding test at 80 °C when using grease no. 1 (containing both zinc carboxylate and a sulfur-type anti-oxidation agent) and grease no. 3 (containing zinc carboxylate but not a sulfur-type anti-oxidation agent). Table 6 lists the amounts of each chemical state obtained by the peak fitting of the results of the XPS analysis. The detected amounts of not only S_{2p} but also Zn_{2p3} were low even when the surface was obtained by a sliding test using grease containing zinc carboxylate. Therefore, the estimated amount of the ZnS tribofilm is significantly low on the composite surface after the test without a sulfur-type anti-oxidation agent. It is indeed necessary to have a source of sulfur to form an adherent ZnS film on the surface of the composite, and there is no adhesion of Zn alone when S is not present, confirming the tribochemistry origin of the presence of Zn and S on the surface of the composite. These results confirm that the contribution of a carboxylates tribofilm on the steel is much greater than the effect of the formation of the ZnS tribofilm on the PA66 surface in terms of the improvement of the tribological properties.

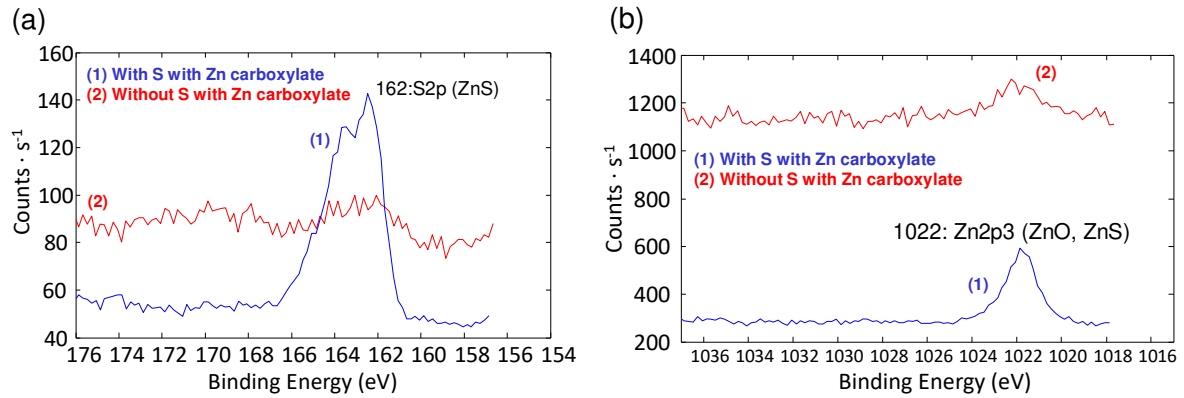


Fig. 33 Results of XPS analysis of the composite surface after 13,000 cycles of a sliding test at 80 °C using grease no. 1 and no. 3: narrow range scanning of (a) S and (b) Zn.

Table 6 Amounts of each chemical state estimated by the curve fitting of the XPS analysis results after 13,000 cycles of a sliding test at 80 °C using grease no. 1 and no. 3.

	162eV S _{2p}	1022eV Zn _{2p3}
With sulfur-type anti-oxidation agent with zinc carboxylate	1.5 at%	1.4 at%
Without sulfur-type anti-oxidation agent with zinc carboxylate	0.1 at%	0.1 at%

The reason for the improvement of the tribological properties through the addition of zinc carboxylate is discussed herein, along with the decreasing effect of the friction coefficient described in Section 3.2. Fig. 34 shows the maximum friction coefficient for each 1 s (the friction coefficient is measured every 0.01 s and the maximum value during each 1 s was extracted) of the sliding test for a stopping time of 200 s at 80 °C when using grease no. 1 and grease no. 2, and GF-reinforced composite. The maximum friction coefficient upon a restart after the 200 s stopping phase is the static coefficient, the value of which is higher than the maximum value of the friction coefficient during the sliding phase over the remaining 9 s. The results indicate that the average values of the static coefficient during the initial 10,000 cycles with or without the addition of zinc carboxylate (grease no. 1 and grease no. 2) are 0.093 and 0.138, respectively. Therefore, the addition of zinc carboxylate decreases the adhesion between the composite and steel during the stopping phase, and the damage of the contact surface after the restart can be decreased. Consequently, the wear and creep of the composite and the wear of the steel counterpart are reduced.

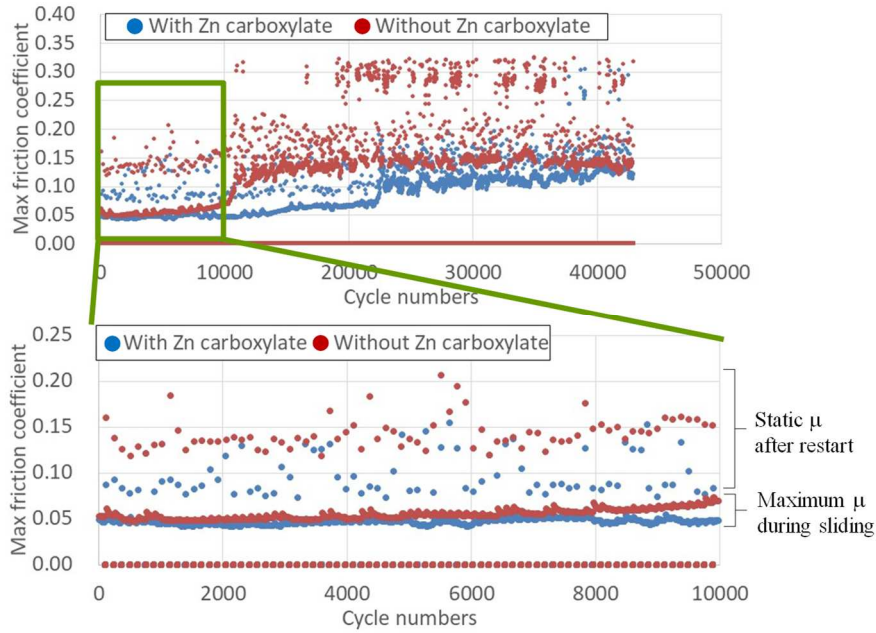


Fig. 34 Evolution of maximum friction coefficient during the sliding tests for a stopping time of 200 s at 80 °C when using grease no. 1 and grease no. 2 and GF-reinforced composite

3.5 Temperature dependence on tribofilm formation

To better understand the effect of temperature on the tribological properties, as presented in Section 3.2, the amounts of Zn and S on the sliding surface of the GF-reinforced PA66 composite after the sliding tests were measured based on SEM-EDX using grease no. 1 (containing both zinc carboxylate and sulfur-type anti-oxidation agent). Fig. 35 shows the SEM and EDX images of Zn and S on the sliding surface after the test for a stopping time of 200 s for different temperatures and cycle numbers. The detected amounts of Zn and S after 13,000 cycles of the test at room temperature are significantly lower, and these results can explain why the addition of zinc carboxylate did not improve the tribological properties at room temperature: We can consider the thermal activation needed for tribochemistry as not being reached during the tests at room temperature. The detected amounts of Zn and S after 5,000 cycles of the sliding test at 120 °C are higher than those at 80 °C for the same numbers of cycles. The presence of Zn and S tribofilms can explain the decrease in the friction coefficient at 120 °C through the addition of zinc carboxylate and a sulfur-type anti-oxidation agent into the grease. However, an improvement in the wear and creep by the addition of zinc carboxylate was not observed, as presented in Section 3.2, because the effect of the degradation in the mechanical properties (the hardness of the sliding surface of the composite, as described in Section 3.2) at 120 °C is considered to be greater than the positive effect of the tribofilm formation. In addition, the transition temperature of carboxylate on the steel surface (iron carboxylate soap), such as laurate, myristate, palmitate, or stearate are 110 °C–140 °C (much higher than the melting point of each fatty acid itself) [34, 50]. Therefore, adhesion between the molecules in the boundary film is diminished and a breakdown of the soap film on the steel is considered to occur by the sliding heat during the test at 100–120 °C, leading to the increase in the wear and creep of the composite as presented in Fig. 6 .

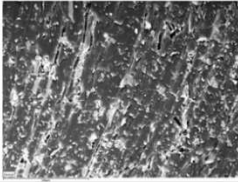


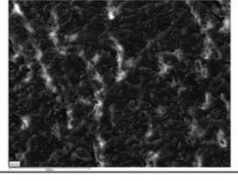
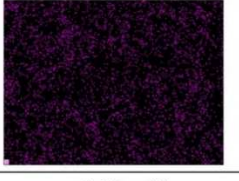

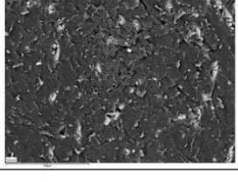
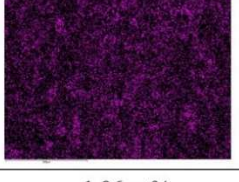
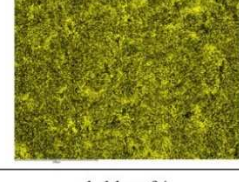
	SEM	Zn	S
RT 13,000 cycles			
	-	0.10 wt%	0.01 wt%
80°C 5,000 cycles			
	-	0.34 wt%	0.47 wt%
120°C 5,000 cycles			
	-	1.06 wt%	1.11 wt%

Fig. 35 SEM and EDX images of Zn and S for different values of temperature and numbers of cycles of the sliding tests for a stopping time of 200 s using grease no.1 and GF-reinforced PA66 composite

3.6 Effects of adding zinc carboxylate to grease on the tribological properties of unreinforced PA66

The effects of adding zinc carboxylate to grease on the tribological properties of unreinforced PA66 were investigated during the sliding test under a stopping time of 1 s (using a temperature increase from the heat generated by sliding). Fig. 36 shows the evolutions of the vertical displacement, the friction coefficient, and the temperature using grease with or without zinc carboxylate (grease no. 1 and grease no. 2). The average friction coefficient during the sliding is 0.050 ± 0.003 with zinc carboxylate and 0.054 ± 0.004 without zinc carboxylate, and a slight effect of the decrease in the friction coefficient is observed. However, the effect of the addition of zinc carboxylate to grease on the decrease in the friction coefficient is much lower than the effect observed in GF-reinforced PA66. In addition, a slight effect from the decrease in temperature was observed by the decrease in the friction coefficient. A gradual increase in creep during the initial phase of the sliding test is observed. However, the proportional increase in the vertical displacement related to the wear, as observed in the GF-reinforced PA66, is not confirmed. Furthermore, a slight effect from the addition of zinc carboxylate on the decrease in the displacement is observed. The height loss after 61,500 cycles of unreinforced PA66 is smaller than the height loss of GF-reinforced PA66. Regardless of the addition of zinc carboxylate to the grease, a wear height loss was not observed, and most of the height loss (80%–95%) was creep. Fig. 37 shows the optical microscope observation of the sliding surface of the unreinforced PA66. A sliding scar was observed in samples with and without zinc carboxylate added to the grease. However, severe wear or a peeling of the surface observed in GF-reinforced PA66 was not observed.

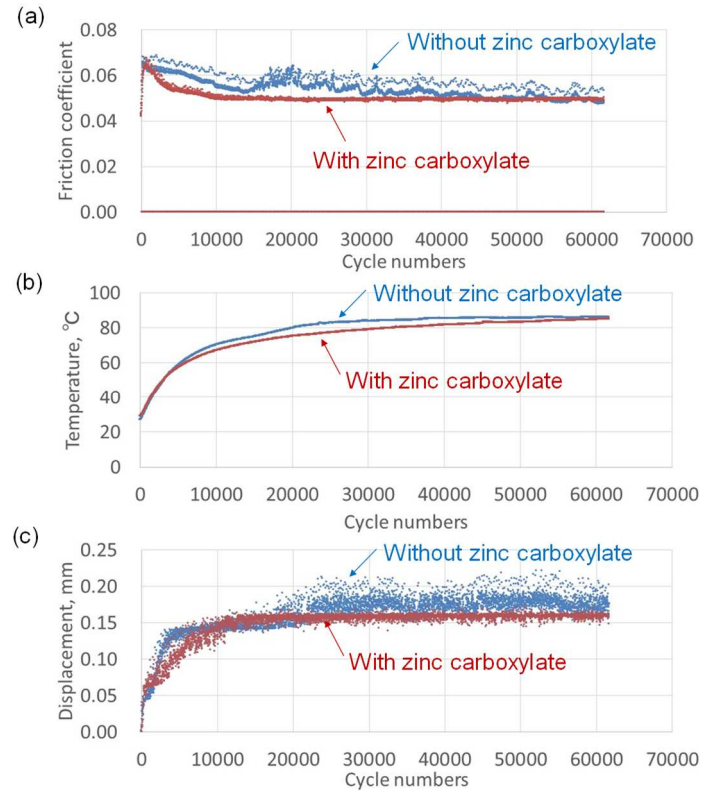


Fig. 36 Evolutions of (a) friction coefficient, (b) temperature, and (c) vertical displacement in the sliding tests with a 1-s stopping phase of unreinforced PA66 with or without zinc carboxylate in grease.

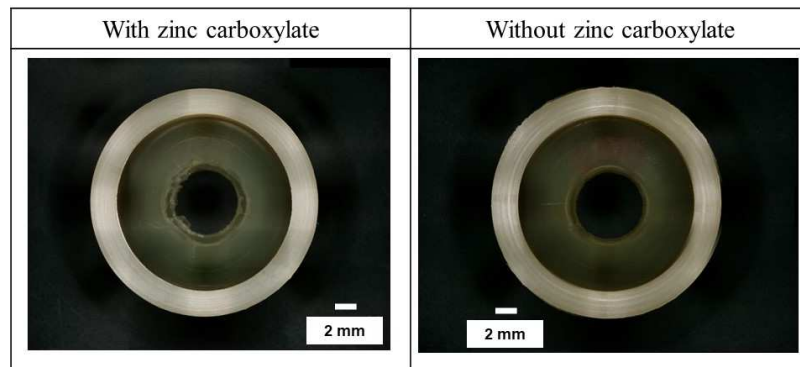


Fig. 37 Optical microscope observations of the sliding surface of unreinforced PA66.

To compare the tribofilm formation between unreinforced PA66 and GF-reinforced PA66, sliding tests under the same conditions as presented in Section 3.3 (at 80 °C, 200 s stopping, for 13,000 cycles) were conducted using grease with or without zinc carboxylate (grease no. 1 and grease no. 2). Fig. 38 shows the evolutions of the friction coefficient and the vertical displacement. A decrease of 11.7% in the average friction coefficient is observed, which is less than the effect in GF-reinforced PA66. In addition, a slight effect of the decrease in displacement is observed. Fig. 39 shows the SEM observation of the steel cylinder after the sliding test when using the grease containing zinc carboxylate. As with the test using GF-reinforced PA66, dark patches can be

seen on the sliding surface. However, the total area of the patches is less than that of the cylinder after the test with a GF-reinforced PA66. Fig. 40 shows the detected amounts of the chemical elements measured by the point analysis of the patches with SEM-EDX, as compared with the amounts on the new steel cylinder, and on the cylinder tested with GF-reinforced PA66 under the same test conditions, as presented in Section 3.3. The proportion of C and O increases and that of Fe decreases compared to the new steel cylinder. However, the detected amounts are smaller than in the results for the test with GF-reinforced PA66, and Zn and S are not detected at all. Considering the results of the ToF-SIMS analysis presented in Section 3.3, a tribofilm of carboxylates composed of hydrocarbon and oxygen was considered to have formed. This difference in the detected amounts of chemical elements and the area of the patches is attributed to the difference in the contact pressure between the PA66 and steel. The Young's modulus of the GF composite is higher than that of the unreinforced PA66 owing to the addition of stiff GF. Therefore, the higher the contact pressure on the sliding test between the GF composite and steel promotes the formation of a tribofilm on the steel surface, and the effect of the decrease in the friction coefficient becomes greater. In addition, Fig. 41 shows an SEM image of the sliding surface of unreinforced PA66 after 13,000 cycles of the sliding test under the same conditions. Fig. 42 shows the detected chemical elements measured using SEM-EDX as compared with the results of the new unreinforced PA66 ring (without sliding test). The results indicate that Zn and S are detected along with Fe related to the wear debris of the steel counterpart, and ZnS tribofilm is considered to have formed on the surface of the unreinforced PA66, similar to the GF-reinforced PA66.

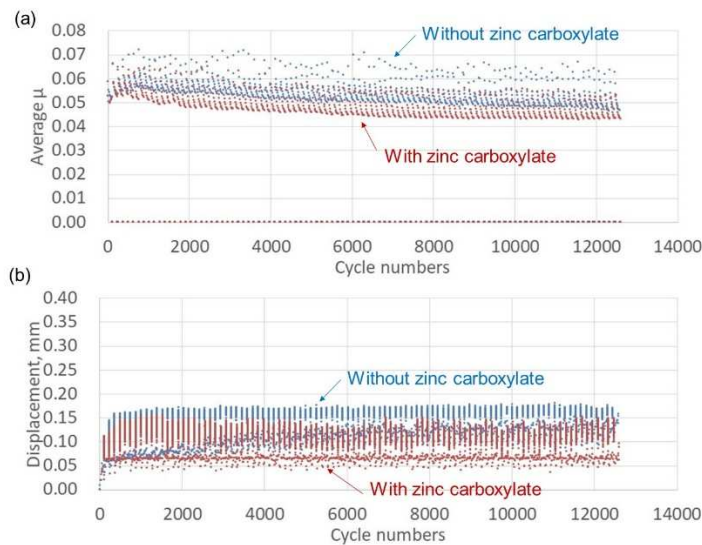


Fig. 38 Evolutions of (a) friction coefficient and (b) vertical displacement during the sliding test at 80 °C, with a 200 s stopping phase of the unreinforced PA66 with or without zinc carboxylate in grease.

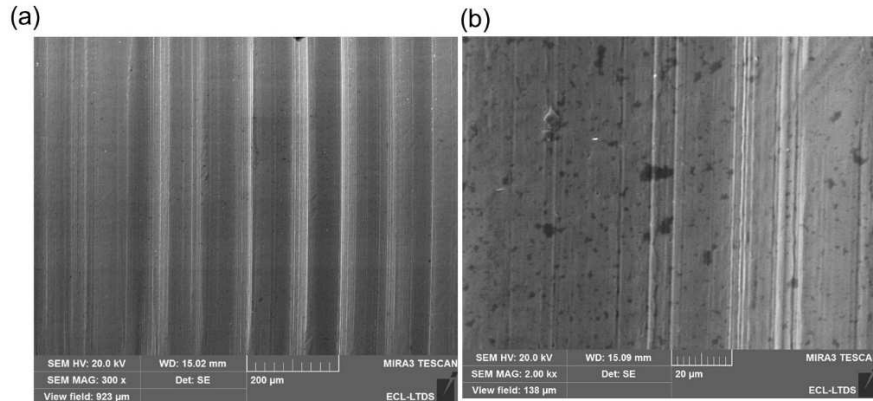


Fig. 39 SEM observations of the steel cylinder after 13,000 cycles of the sliding test with unreinforced PA66 with grease containing zinc carboxylate (grease no. 1) (a) at a magnification of $\times 300$: (b) at a magnification of $\times 2000$.

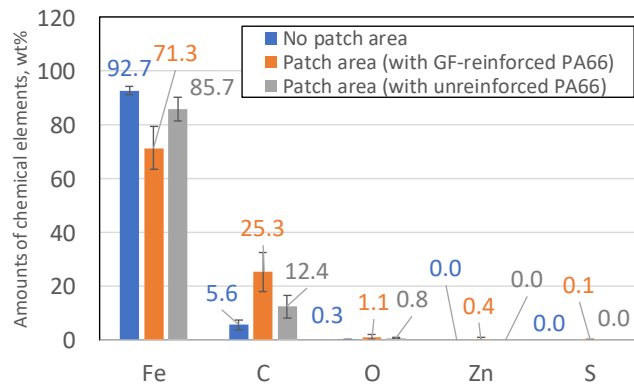


Fig. 40 Detected amounts of chemical elements of the steel cylinder after 13,000 cycles of the sliding test with unreinforced PA66 with grease containing zinc carboxylate (grease no. 1) measured using SEM-EDX (average value of three different analyses).

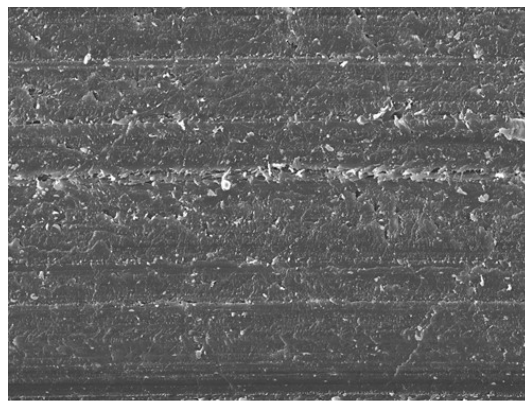


Fig. 41 SEM observation of the sliding surface of unreinforced PA66 ring after 13,000 cycles of the sliding test at 80 °C with 200-s stopping phase with zinc carboxylate added to the grease (grease no. 1).

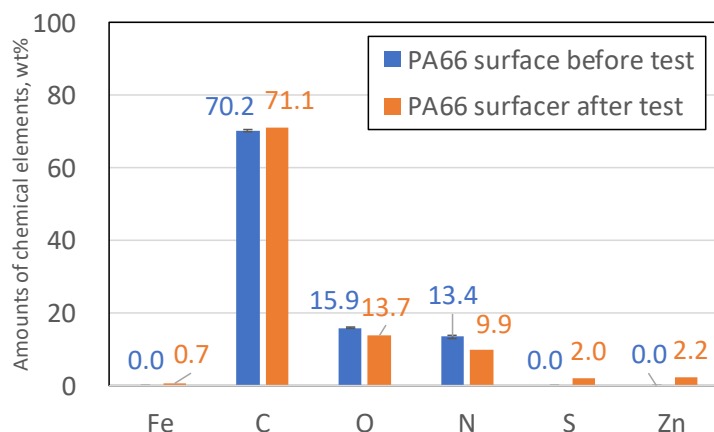


Fig. 42 Amounts of chemical element on the surface of PA66 before/after 13,000 cycles of the sliding test at 80 °C with 200 s stopping phase with zinc carboxylate added grease (grease no. 1) as measured using SEM-EDX (average value of three different analyses).

4. Conclusions

The effects of temperature and the addition of zinc carboxylate to grease on the tribological properties of PA66 in contact with carbon steel were clarified. The tribological properties can be described by considering the temperature dependence of both the mechanical properties of PA66 and the tribochemistry. The following points have been highlighted.

- 1) Wear and creep resistance of GF-reinforced PA66 deteriorated with an increase in temperature using grease without the addition of zinc carboxylate. This can be explained by the temperature dependence of the mechanical properties on the sliding surface of the composite (hardness and Young's modulus) as measured based on the micro indentation procedure.
- 2) The effects of the addition of zinc carboxylate were investigated at each temperature. The effects of the improvement of the tribological properties were not observed at room temperature. Significant effects of the addition of zinc carboxylate in the grease, such as a decrease in the friction coefficient, a decrease in the wear and creep of the composite, and a decrease in the wear of the steel counterpart, were observed at 80 °C. The decrease in the friction coefficient was observed at 120 °C. However, the effect of the decrease in the wear and creep was not confirmed.
- 3) A ToF-SIMS analysis of the steel surface after the sliding test at 80 °C revealed the formation of a heterogeneous tribofilm composed of carboxylates. An XPS analysis of the GF-reinforced PA66 composite surface showed the presence of a ZnS reactive tribofilm related to the tribochemical reaction between zinc carboxylate and sulfur-type anti-oxidation agent.
- 4) The contribution of the formation of the carboxylates tribofilm on the steel surface in the improvement of

the tribological properties is greater than that of the formation of a ZnS tribofilm on the PA66 surface.

Acknowledgment

The ToF-SIMS analyses were conducted at Science et Surface (<https://www.science-et-surface.fr/>).

References

- [1] S. Kamerling, A. K. Schlarb, Magnesium hydroxide — A new lever for increasing the performance and reliability of PA66/steel tribosystems, *Tribol. Int.* 147 (2020) 106271. <https://doi.org/10.1016/j.triboint.2020.106271>
- [2] S.M. Lee, M.W. Shin, H. Jangn, Effect of carbon-nanotube length on friction and wear of polyamide 6,6 nanocomposites, *Wear* 320 (2014) 103-110. <https://doi.org/10.1016/j.wear.2014.08.011>
- [3] M.T. Lates, R. Velicu, C.C. Gavrilă, Temperature, pressure, and velocity influence on the tribological properties of PA66 and PA46 Polyamides, *Materials* 12 (20) (2019) 3452. <https://doi.org/10.3390/ma12203452>
- [4] D.W. Gebretsadik, J. Hardell, B.P. Rakash, Friction and wear characteristics of PA 66 polymer composite/316L stainless steel tribopair in aqueous solution with different salt levels, *Tribol. Int.* 141 (2020) 105917. <https://doi.org/10.1016/j.triboint.2019.105917>
- [5] J. Chen, H. Xu, C. Liu, L. Mi, C. Shen, The effect of double grafted interface layer on the properties of carbon fiber reinforced polyamide 66 composites. *Composites Sci. and Technol.* 168 (2018) 20-27. <https://doi.org/10.1016/j.compscitech.2018.09.007>
- [6] S. Senthilvelan, R. Gnanamoorthy, Damage Mechanisms in injection molded unreinforced, glass and carbon reinforced nylon 66 spur gears, *Appl. Compos. Mater.* 11 (2004) 377–397. <https://doi.org/10.1023/B:ACMA.0000045313.47841.4e>
- [7] B. Sarita, S. Senthilvelan, Effects of lubricant on the surface durability of an injection molded polyamide 66 spur gear paired with a steel gear, *Tribol. Int.* 137 (2019) 193–211. <https://doi.org/10.1016/j.triboint.2019.02.050>
- [8] S. Senthilvelan, R. Gnanamoorthy, Fiber reinforcement in injection molded nylon 6/6 spur gears, *Appl. Compos. Mater.* 13 (2006) 237–248. <https://doi.org/10.1007/s10443-006-9016-9>
- [9] J. Tavčar, G. Grkman, J. Duhovnik, Accelerated lifetime testing of reinforced polymer gears, *J. of Advanced Mec. Des., Sys., and Man.* 12 (2018) 1-13. <https://doi.org/10.1299/jamdsm.2018jamdsm0006>
- [10] Y. Zhang, C. Pursell, K. Mao, S. Leigh, A physical investigation of wear and thermal characteristics of 3D printed nylon spur gears. *Tribol. Int.*, 141 (2020) 105953. <https://doi.org/10.1016/j.triboint.2019.105953>
- [11] M. Kurokawa, Y. Uchiyama, T. Iwai, S. Nagai, Performance of plastic gear made of carbon fiber reinforced polyamide 12, *Wear* 254 (2003) 468–473. [https://doi.org/10.1016/S0043-1648\(03\)00020-6](https://doi.org/10.1016/S0043-1648(03)00020-6)
- [12] S. Kirupasankar, C. Gurunathan, R. Gnanamoorthy, Transmission efficiency of polyamide nanocomposite spur gears, *Mater. Des.* 39 (2012) 338-343. <https://doi.org/10.1016/j.matdes.2012.02.045>
- [13] D. Scott, J. Blackwell, P.J. McCullagh, G.H. Mills, Composite materials for rolling bearing cages, *Wear* 15 (1970) 257-269. [https://doi.org/10.1016/0043-1648\(70\)90016-5](https://doi.org/10.1016/0043-1648(70)90016-5)
- [14] H. Oh, M.H. Azarian, C. Morillo, M. Pecht, E. Rhem, Failure mechanisms of ball bearings under lightly loaded, non-accelerated usage conditions, *Tribol. Int.* 81 (2015) 291–299.

<https://doi.org/10.1016/j.triboint.2014.09.014>

- [15] J. Kohout, Strength changes of moulded polyamide composite caused by thermal oxidation, *J. of Mat. Sci.* 34 (1999) 843-849. <https://doi.org/10.1023/A:1004593417901>
- [16] Y.K. Chen, O.P. Modi, A.S. Mhay, A. Chrysanthou, J.M. O'Sullivan, The effect of different metallic counterface materials and different surface treatments on the wear and friction of polyamide 66 and its composite in rolling-sliding contact, *Wear* 255 (2003) 714–721. [https://doi.org/10.1016/S0043-1648\(03\)00054-1](https://doi.org/10.1016/S0043-1648(03)00054-1)
- [17] Q. Guo, W. Luo, Mechanisms of fretting wear resistance in terms of material structures for unfilled engineering polymers, *Wear* 249 (2002) 924-931. [https://doi.org/10.1016/S0043-1648\(01\)00827-4](https://doi.org/10.1016/S0043-1648(01)00827-4)
- [18] B. Pan, S Zhang, W Li, J Zhao, J Liu, Y Zhang, Y Zhang, Tribological and mechanical investigation of MC nylon reinforced by modified graphene oxide, *Wear* 294-295 (2012) 395-401. <https://doi.org/10.1016/j.wear.2012.07.032>
- [19] S.N. Kukureka, C.J. Hooke, M. Rao, P. Liao, Y. K. Chen, The effect of fibre reinforcement on the friction and wear of polyamide 66 under dry rolling–sliding contact, *Tribol. Int.* 32 (1999) 107–116. [https://doi.org/10.1016/S0301-679X\(99\)00017-1](https://doi.org/10.1016/S0301-679X(99)00017-1)
- [20] S. Zhou, Q. Zhang, C. Wu, J. Huang, Effect of carbon fiber reinforcement on the mechanical and tribological properties of polyamide6/polyphenylene sulfide composites, *Mater. Des.* 44 (2013) 493–499. <https://doi.org/10.1016/j.matdes.2012.08.029>
- [21] D.H. Gordon, S.N. Kukureka, The wear and friction of polyamide 46 and polyamide 46/aramid-fibre composites in sliding-rolling contact, *Wear* 267 (2009) 669–678. <https://doi.org/10.1016/j.wear.2008.11.026>
- [22] S. S. Kim, M. W. Shin, H. Jang, Tribological properties of short glass fiber reinforced polyamide 12 sliding on medium carbon steel, *Wear* 274-275 (2012) 34-42. <https://doi.org/10.1016/j.wear.2011.08.009>
- [23] M.W. Shin, S.S. Kim, H. Jang, Friction and wear of polyamide 66 with different weight average molar mass, *Tribol. Lett.* 44 (2011) 151–158. <https://doi.org/10.1007/s11249-011-9833-3>
- [24] J.W. Kim, H. Jang, Jin Woo Kim, Friction and wear of monolithic and glass-fiber reinforced PA66 in humid conditions, *Wear* 309 (2014) 82-88. <https://doi.org/10.1016/j.triboint.2019.105917>
- [25] G.H. Kim, J.W. Lee, T.II. Seo, Durability characteristics analysis of plastic worm wheel with glass fiber reinforced polyamide, *Materials* 6 (2013) 1873–1890. <https://doi.org/10.3390/ma6051873>
- [26] H. C. Ahn, Wear of glass fiber reinforced polyamide worm gear according to the direction of the glass fiber, Technical paper presented at SAE 2010 World Congress & Exhibition. <https://doi.org/10.4271/2010-01-0917>
- [27] T. Kunishima, K. Miyake, T. Kurokawa, H. Arai, Clarification of tribological behavior on tooth surface of resin worm gear for electric power steering, *JTEKT Eng. J. English Edition*, 1013E (2016) 27–33.
- [28] T. Kunishima, T. Kurokawa, H. Arai, V. Fridrici, P. Kapsa, Reactive extrusion mechanism, mechanical and tribological behavior of fiber reinforced polyamide 66 with added carbodiimide, *Mater. Des.* 188 (2020) 108447. <https://doi.org/10.1016/j.matdes.2019.108447>
- [29] A. Bormuth, J. Zuleeg, C. Schmitz, R. Schmitz, M. Pfadt and H. Meven, Lubrication of plastic worm gears, *Power Transmission Eng. Aug.* (2019) 42-47.
- [30] T. Kochi, R. Ichimura, M. Yoshihara, D. Dong, Y. Kimura, Film thickness and traction in soft EHL with grease, *Tribology online* 12 (4) (2017) 171-176. <https://doi.org/10.2474/trol.12.171>

- [31] M. Kurokawa, Y. Uchiyama, S. Nagai, Performance of plastic gear made of carbon fiber reinforced poly-ether-ether-ketone, *Tribol. Int.* 32 (1999) 491-497. [https://doi.org/10.1016/S0301-679X\(99\)00078-X](https://doi.org/10.1016/S0301-679X(99)00078-X)
- [32] L. R. Rudnick, *Lubricant additives chemistry and applications second editions*, (2017) 594-597.
- [33] D. Evans, J. B. Matthews, The structure of aluminum stearate grease, *J. Colloid Sci.* 9 1 (1954) 60-69. [https://doi.org/10.1016/0095-8522\(54\)90086-0](https://doi.org/10.1016/0095-8522(54)90086-0)
- [34] B. Bhushan, *Introduction of Tribology second edition*, (2013) 508-510.
- [35] A. Adhvaryu, C. Sung, S.Z. Erhan, Fatty acids and antioxidant effects on grease microstructures, *Industrial Crops and Products* 21 3 (2005) 285-291. <https://doi.org/10.1016/j.indcrop.2004.03.003>
- [36] N. Kumar, V. Saini, J. Bijwe, Performance properties of lithium greases with PTFE particles as additive: Controlling parameter- size or shape?, *Tribol. Int.*, 148 (2020) 106302. <https://doi.org/10.1016/j.triboint.2020.106302>
- [37] R. G. Duque, Z. Wang, D. Duell, D. E. Fowler, ToF-SIMS analysis of anti-fretting films generated on the surface of ball bearings containing dithiocarbamate and dithiophosphate grease additives, *Applied Surface Sci.* 231-232 (2004) 342-347. <https://doi.org/10.1016/j.apsusc.2004.03.088>
- [38] R. Lu, M. Morimoto, H. Tani, N. Tagawa, S. Koganezawa, Tribological properties of alkylidiphenylethers in boundary lubrication, *Lubricants* (2019) 7, 112. <https://doi.org/10.3390/lubricants7120112>
- [39] J. Shu, K. Harris, B. Munavirov, R. Westbroek, J. Leckner, S. Glavatskih, Tribology of polypropylene and Li-complex greases with ZDDP and MoDTC additives, *Tribol. Int.*, 118 (2018) 189-195. <https://doi.org/10.1016/j.triboint.2017.09.028>
- [40] M. Miyajima, K. Kitamura, K. Matsumoto, Characterization of tribochemical reactions on steel surfaces, *Nippon steel & Sumitomo metal tech. rep.*, 114 (2017) 101-107.
- [41] R. Nakata, Grease lubrication technology for sliding automobile parts, *JTEKT Eng. J. English Edition*, 1011E (2014) 25-30.
- [42] T. Kunishima, Y. Nagai, T. Kurokawa, G. Bouvard, J-C. Abry, V. Fridrici, P. Kapsa, Tribological behavior of glass fiber reinforced-PA66 in contact with carbon steel under high contact pressure, sliding and grease lubricated conditions, *Wear* (2020). <https://doi.org/10.1016/j.wear.2020.203383>
- [43] R. Rabe, J-M. Breguet, P. Schwaller, S. Stauss, F-J. Haug, J. Patscheider, J. Michler, Observation of fracture and plastic deformation during indentation and scratching inside the scanning electron microscope. *Thin Solid Films* 469-470 (2004) 206-213. <https://doi.org/10.1016/j.tsf.2004.08.096>
- [44] J.M. Wheeler, J. Michler, Elevated temperature, nano-mechanical testing in situ in the scanning electron microscope. *Review of Scientific Instruments* 84 (2013) 045103. <https://doi.org/10.1063/1.4795829>
- [45] W.C. Oliver, G.M. Pharr, An improved technique for determining hardness and elastic-modulus using load and displacement sensing indentation experiments. *J. Materials Research* 7 (1992) 1564-1583. <https://doi.org/10.1557/JMR.1992.1564>
- [46] B.N. Lucas, W.C. Oliver, G.M. Pharr, J-L. Loubet, Time dependent deformation during indentation testing. *Proceedings of the 1996 MRS Spring Meeting, April 8, 1996 - April 12, 1996, vol. 436, San Francisco, CA, USA: (1996) 233-238.*
- [47] A.H.W. Ngan, B. Tang, Viscoelastic effects during unloading in depth-sensing indentation. *J. Mater.*

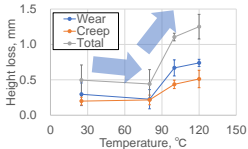
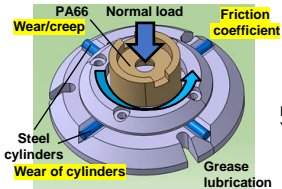
Research 17 (2002) 2604–2610. <https://doi.org/10.1557/JMR.2002.0377>

[48] K. Laajalehto, I. Kartio, P. Nowak, XPS study of clean metal sulfide surfaces, *Applied Surface Sci.*, 81 (1994) 11-15. [https://doi.org/10.1016/0169-4332\(94\)90080-9](https://doi.org/10.1016/0169-4332(94)90080-9)

[49] X. Deng, D.C. Sorescu, J. Lee, Single-layer ZnS supported on Au (111): A combined XPS, LEED, STM and DFT study, *Surface Sci.*, 658 (2017) 9-14. <https://doi.org/10.1016/j.susc.2016.12.003>

[50] S. Loehlé, C. Matta, C. Minfray, T. LeMogne, R. Iovine, Y. Obara, A. Miyamoto, J.M. Martin, Mixed lubrication of steel by C18 fatty acids revisited. Part I: Toward the formation of carboxylate, *Tribology International* 82 (2015) 218-227. <https://doi.org/10.1016/j.triboint.2014.10.020>

<Tribological properties>

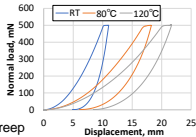


<Mechanical properties>

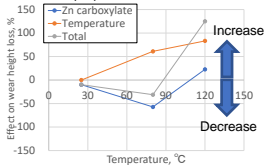
Micro indentation



Hardness \Rightarrow Wear
Young's modulus \Rightarrow Creep



Contribution of zinc carboxylate in grease and mechanical properties



<Tribochemistry>

